msp

Geometry & Topology 24 (2020) 2075–2125

Floer homology, group orderability, and taut foliations of hyperbolic 3–manifolds

NATHAN M DUNFIELD

This paper explores the conjecture that the following are equivalent for irreducible rational homology 3–spheres: having left-orderable fundamental group, having nonminimal Heegaard Floer homology, and admitting a coorientable taut foliation. In particular, it adds further evidence in favor of this conjecture by studying these three properties for more than 300 000 hyperbolic rational homology 3–spheres. New or much improved methods for studying each of these properties form the bulk of the paper, including a new combinatorial criterion, called a foliar orientation, for showing that a 3–manifold has a taut foliation.

57M27; 20F60, 20M05, 57M05, 57M50, 57R30, 57R58

Published: 10 November 2020 DOI: 10.2140/gt.2020.24.2075

1 Introduction

1.1 The motivating conjecture

Throughout this introduction, please see Section 2 for precise definitions and conventions, which include that all 3–manifolds are orientable and all foliations are coorientable. This paper explores the following:

1.2 Conjecture *For an irreducible $\mathbb{Q}$–homology 3–sphere Y, the following are equivalent*:

(1) *Y is orderable, ie its fundamental group $\pi_1(Y)$ is left-orderable.*

(2) *Y is not an L–space, ie its Heegaard Floer homology is not minimal.*

(3) *Y admits a taut foliation.*

The equivalence of (1) and (2) was boldly postulated by Boyer, Gordon, and Watson in [7], which includes a detailed discussion of this conjecture. The equivalence of (2) and (3) was formulated as a question by Ozsváth and Szabó after they proved that (3) implies (2) — see Bowden [5], Kazez and Roberts [53], and Ozsváth and Szabó [62] — and upgraded to a conjecture by Juhász [52]. On its face, Conjecture 1.2 is quite surprising given the disparate nature of these three conditions, but there are actually a number of interconnections between them, summarized in Figure 1. Despite much initial skepticism, substantial evidence has accumulated in favor of Conjecture 1.2. For example, it holds for *all* graph manifolds — see Boyer and Clay [6], Hanselman, Rasmussen, Rasmussen, and Watson [42], and Rasmussen [65] — and for many branched covers of knots in the 3–sphere — see Gordon and Lidman [39] — as well as for certain families of Dehn surgeries on a fixed manifold — see Culler and myself [19]. Here, despite my best efforts to disprove this conjecture, I add to this evidence by exploring these properties for more than 300 000 hyperbolic rational homology 3–spheres.

This was challenging in part because the property in (1) is not known to be algorithmically decidable (and it is undecidable in the broader category of all finitely presented groups), and while property (3) is known to be algorithmically decidable, the current algorithm is believed by its authors to be "nearly impossible to implement on a computer"; see Agol and Li [2]. The bulk of this paper is devoted to giving new or much improved methods for exploring all three of these properties; see Sections 1.7–1.10 for an overview. However, let me first describe Theorem 1.6, which is the main result here supporting Conjecture 1.2.

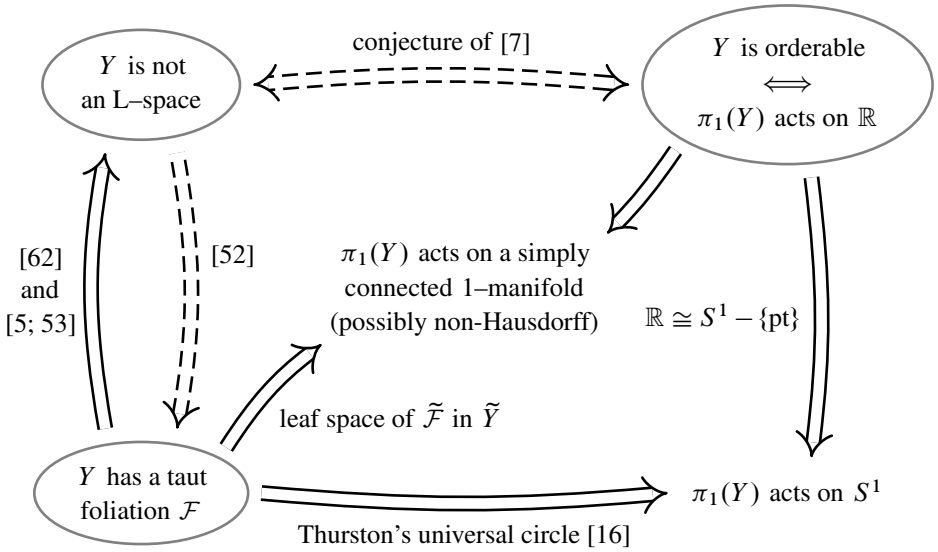

Figure 1: Some results related to Conjecture 1.2, which asserts the equivalence of the three circled conditions. Here Y is an irreducible $\mathbb{Q}$–homology 3–sphere, all foliations are coorientable, and all actions are nontrivial, faithful, and orientation-preserving; the solid arrows are theorems and dotted ones conjectures. See [7] for a complete discussion. This figure is copied from [19].

1.3 A few rational homology 3–spheres

Here I consider a census, denoted by $\mathcal{Y}$, of some 307 301 rational homology 3–spheres which are described in Section 3.2. Each manifold in $\mathcal{Y}$ is a Dehn filling of a 1–cusped hyperbolic 3–manifold that can be triangulated with at most 9 ideal tetrahedra; the latter were enumerated by Burton [12].

1.4 Theorem *The rational homology 3–spheres in $\mathcal{Y}$ are all hyperbolic and distinct.*

Additionally, I have strong numerical evidence that the systole, that is, the length of the shortest closed geodesic, is at least 0.2 for all manifolds in $\mathcal{Y}$. In fact, I conjecture that $\mathcal{Y}$ is precisely the set of all hyperbolic rational homology 3–spheres that are Dehn fillings on 1–cusped manifolds from [12] where the systole is at least 0.2.

For comparison, the Hodgson–Weeks census consists of 11 031 closed hyperbolic 3–manifolds with systole at least 0.3 that are Dehn fillings on manifolds triangulated by at most 7 ideal tetrahedra [46]. In particular, the census $\mathcal{Y}$ contains the 10 903 rational homology 3–spheres in the Hodgson–Weeks census, and those make up 3.5% of its total.

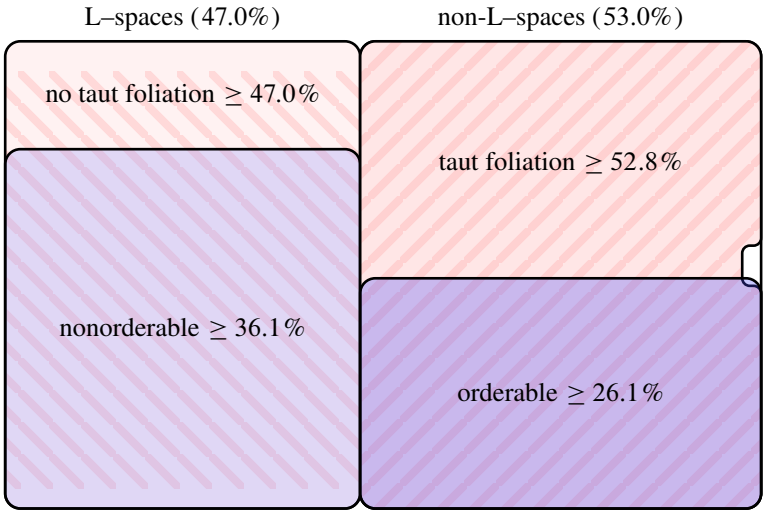

Figure 2: A visual summary of what Theorem 1.6 says about the rational homology 3–spheres in $\mathcal{Y}$. In particular, Conjecture 1.2 holds in full for the 62.2% of $\mathcal{Y}$ corresponding to the lowest two regions above. Moreover, the equivalence of parts (2) and (3) in the conjecture holds for 99.8% of $\mathcal{Y}$, namely everything except the notch on the middle of the right side.

1.5 Overall results

The main result of this paper supporting Conjecture 1.2 is the following, which is summarized in Figure 2.

1.6 Theorem *Of the* 307 301 *hyperbolic rational homology* 3*–spheres in* $\mathcal{Y}$:

(1) *Exactly* 144 298 (47.0%) *are L–spaces and* 163 003 (53.0%) *are non-L–spaces.*

(2) *At least* 162 341 (52.8%) *of these manifolds admit taut foliations*; *this is* 99.6% *of the non-L–spaces.*

(3) *At least* 80 236 (26.1%) *of these manifolds are orderable*; *all of the known orderable manifolds are non-L–spaces.*

(4) *At least* 110 940 (36.1%) *of these manifolds are not orderable*; *all of the known nonorderable manifolds are L–spaces.*

Overall, *Conjecture 1.2 holds for at least* 191 089 (62.2%) *of these manifolds.*

I now turn to summarizing the techniques used to prove this theorem, which form the real heart of the paper.

1.7 Constructing foliations

In Section 7, I give a new purely combinatorial technique for constructing a taut foliation on a closed 3–manifold Y: a *foliar orientation* of the edges of a triangulation $\mathcal{T}$ for Y. This notion is a strengthening of the local orientation of Calegari [14], and a foliar orientation has an associated branched surface which is a canonical smoothing of the 2–skeleton of the dual cell complex to $\mathcal{T}$. Li's theory of laminar branched surfaces [55] turns out to apply to this branched surface, showing that it carries a lamination that can be extended to a taut foliation of Y; see Theorems 7.1 and 7.6 for more. Such foliar orientations turn out to be extraordinarily common, occurring for more than 160 000 of the manifolds in $\mathcal{Y}$ by Theorem 7.4 and providing the bulk of the proof of Theorem 1.6(2). It is unclear whether every taut foliation arises from a foliar orientation on some triangulation; see Remark 7.8 for some possible approaches to this question.

The closely related notation of a *persistently foliar orientation* on an ideal triangulation of a compact 3–manifold M whose boundary is a torus is introduced in Section 8. Theorem 8.1 shows that having a persistently foliar orientation means that all but at most one Dehn filling on M has a taut foliation. In addition to being used in the proof of Theorem 1.6(2), persistently foliar orientations are ubiquitous on the exteriors of knots in S^3:

8.3 Theorem *Among the* 1 210 608 *nonalternating prime knots with at most* 16 *crossings, there are exactly* 12 *that are L–space knots. All the others have ideal triangulations of their exteriors with persistently foliar orientations; in particular, any nontrivial Dehn surgery on one of these knots admits a coorientable taut foliation.*

Motivated by this and the work of Delman and Roberts [22] in the case of alternating knots, I posit in Conjecture 8.4 that the exterior of a non-L–space knot in S^3 always has a persistently foliar branched surface.

1.8 Nonorderability and the word problem

For the orderability of Y, I used three separate techniques. The first of these, described in Section 5, is a method for showing that $\pi_1(Y)$ is *not* left-orderable. The basic approach follows Calegari and myself [16, Sections 8–10], but with the key change of how the word problem is solved in $\pi_1(Y)$. Rather than using the theory of automatic groups, I use a new approach specific to the fundamental group of a finite-volume hyperbolic 3–manifold Y. The idea is to use a numerical approximation of the holonomy

representation $\pi_1(Y) \to \mathrm{PSL}_2\mathbb{C}$ that has been rigorously verified as correct to within some small tolerance via the interval analysis method of Hoffman, Ichihara, Kashiwagi, Masai, Oishi, and Takayasu [47]. See Section 6 for details.

1.9 Orderability via foliations and $\widetilde{\mathrm{PSL}_2\mathbb{R}}$

The remaining techniques for studying orderability were a pair of independent methods for showing Y is orderable. The first uses taut foliations, specifically the fact that if Y has a taut foliation $\mathcal{F}$ whose Euler class $e(\mathcal{F}) \in H^2(Y;\mathbb{Z})$ vanishes then Y is orderable; see Boyer and Hu [8, Theorem 8.1]. Section 9 explains how to calculate $e(\mathcal{F})$ when $\mathcal{F}$ comes from a foliar orientation, and then uses this to show some 32 347 of the manifolds in $\mathcal{Y}$ are orderable in Theorem 9.3.

The second technique for showing orderability is the much-used method of finding a nontrivial representation $\widetilde{\rho}\colon \pi_1(Y) \to \widetilde{\mathrm{PSL}_2\mathbb{R}}$; see [19] and the historical discussion therein for many prior examples of this. The new feature is that I prove the existence of $\widetilde{\rho}$ using interval analysis in the same spirit as [47]. The fact that $\widetilde{\mathrm{PSL}_2\mathbb{R}}$ is nonlinear complicates matters somewhat as you will see in Section 11, but in the end I successfully applied it to 64 180 manifolds in Theorem 10.1.

The starting point for Theorem 10.1 was a numerical study of representations of $\pi_1(Y)$ to $\mathrm{SL}_2\mathbb{C}$ for all the Y in $\mathcal{Y}$ which is described in Section 10. There, using Ptolemy coordinates and numerical algebraic geometry, I found compelling evidence of 27.8 million such representations, summarized in Table 3. One interesting observation, given the importance of $\widetilde{\mathrm{PSL}_2\mathbb{R}}$–representations in earlier work on Conjecture 1.2, is that the L–spaces actually had more representations to $\mathrm{SL}_2\mathbb{R}$ than the non-L–spaces. In fact, if the Euler classes of the $\mathrm{SL}_2\mathbb{R}$–representations found were simply random elements of $H^2(Y;\mathbb{Z})$, you would expect $\mathcal{Y}$ to contain about 6000 counterexamples to Conjecture 1.2 (see Remark 10.7). This allows us to reject the hypothesis that these Euler classes are random with $p = 10^{-2700}$, providing yet more evidence for Conjecture 1.2.

1.10 Computing Floer homology

The property of being an L–space is algorithmically decidable, by Sarkar and Wang [68]. Moreover, the bordered Heegaard Floer theory of Lipshitz, Ozsváth, and Thurston [57; 56] provides powerful and effective computational tools for determining this. However, rather than attacking the problem head on, I chose to use a bootstrapping

procedure that exploited the structure of the big Dehn surgery graph — see Hoffman and Walsh [48] — via the results of Rasmussen and Rasmussen [64] on L–space Dehn fillings.

Suppose M is a compact 3–manifold with ∂M a torus. When M has two Dehn fillings that are L–spaces it is *Floer simple*, and Rasmussen and Rasmussen show in [64] how to completely determine which Dehn fillings are L–spaces by using essentially only the ordinary Alexander polynomial. By definition, the manifolds in $\mathcal{Y}$ are Dehn fillings on a collection $\mathcal{C}$ of manifolds with torus boundary, and many manifolds in $\mathcal{Y}$ have multiple such descriptions. Starting with the complete list of all exceptional Dehn fillings on $\mathcal{C}$ provided by my previous paper [23], I applied the definition to see that almost 20% of the manifolds in $\mathcal{C}$ are Floer simple. Then the results of [64] determine the L–space status of all Dehn fillings on those manifolds, in particular showing that almost 8% of $\mathcal{Y}$ are L–spaces. This in turn shows that even more manifolds in $\mathcal{C}$ are Floer simple. Repeating this and several related deductions, I eventually recovered the complete picture of which manifolds in $\mathcal{Y}$ are L–spaces. See Section 4 for details and Table 1 for a summary.

1.11 Code and data

The proof of Theorem 1.6 above is of course heavily computer-assisted. Moreover, discovering it took many CPU-decades of computational time, quite possibly several CPU-centuries, using a computer cluster with a few hundred processor cores. However, checking the final proof is much faster. For example, it is quick to check that a saved edge orientation of a particular triangulation is foliar, but much time can be spent searching through triangulations and orientations in hopes of finding such an object in the first place. Complete code and all associated data has been archived at [24]; see Section 12 for details.

1.12 Open questions and next steps

For interesting specific examples, open questions, and avenues for further research, see Section 3.2, Remarks 3.4, 4.9, 5.6, 7.8, 8.10, 9.4, and 9.5, Conjecture 8.4, and Question 8.7.

1.13 History and acknowledgements

I began the first iteration of this project in 2004 not long after [54] appeared on the arXiv and have worked on it on and off since, slowly increasing both the size of

the sample and the range of techniques, always seeking a counterexample to what is now Conjecture 1.2. Thus I cannot give here a complete accounting of the debts I owe both individuals and institutions on this project. Certainly, I gratefully thank Ian Agol, John Berge, Danny Calegari, Marc Culler, Jake Rasmussen, Rachel Roberts, Saul Schleimer, and Liam Watson for many helpful conversations and ideas. This work was done at Caltech, the University of Illinois, ICERM, the University of Melbourne, and IAS, and was funded in part by the Sloan Foundation, the Simons Foundation, and the US National Science Foundation, the latter most recently by the GEAR Network (DMS-1107452), DMS-1510204, and DMS-1811156. Finally, I thank the referees for their helpful comments.

2 Terminology and conventions

All 3–manifolds will be orientable, all foliations coorientable, and all group actions on manifolds will be orientation-preserving. A $\mathbb{Q}$–homology 3–sphere is a closed 3–manifold whose rational homology is the same as that of S^3. A $\mathbb{Q}$–homology solid torus is a compact 3–manifold M with boundary a torus where $H_*(M;\mathbb{Q}) \cong H_*(D^2 \times S^1;\mathbb{Q})$; this is equivalent to M being the exterior of a knot in some $\mathbb{Q}$–homology 3–sphere. One defines $\mathbb{Z}$–homology 3–spheres and solid tori analogously.

Suppose M is a compact 3–manifold with ∂M a torus. A *slope* on ∂M is an unoriented isotopy class of simple closed curves or, equivalently, a primitive element of $H_1(\partial M;\mathbb{Z})$ modulo sign. The set of all slopes will be denoted by $Sl(M)$, which can be viewed as the rational points in the projective line $P^1(H_1(\partial M;\mathbb{R})) \cong P^1(\mathbb{R})$. The Dehn fillings of M are parametrized by $\alpha \in Sl(M)$, with $M(\alpha)$ being the Dehn filling where α bounds a disk in the attached solid torus. When the interior of M is hyperbolic, Thurston showed that all but finitely many $M(\alpha)$ are also hyperbolic [73]. The nonhyperbolic Dehn fillings are called *exceptional*, and the corresponding slopes the *exceptional slopes*.

A group is called *left-orderable* when it admits a total ordering that is invariant under left multiplication (see [18] for an introduction to the role of orderable groups in topology). We will say that a closed 3–manifold Y is *orderable* when $\pi_1(Y)$ is left-orderable. By convention, the trivial group is not left-orderable, and so S^3 is not orderable.

Heegaard Floer homology will always have coefficients in $\mathbb{F}_2 = \mathbb{Z}/2\mathbb{Z}$. Recall from [63] that an *L–space* is a $\mathbb{Q}$–homology 3–sphere with minimal Heegaard Floer homology, specifically one where $\dim \widehat{\mathrm{HF}}(Y) = |H_1(Y;\mathbb{Z})|$.

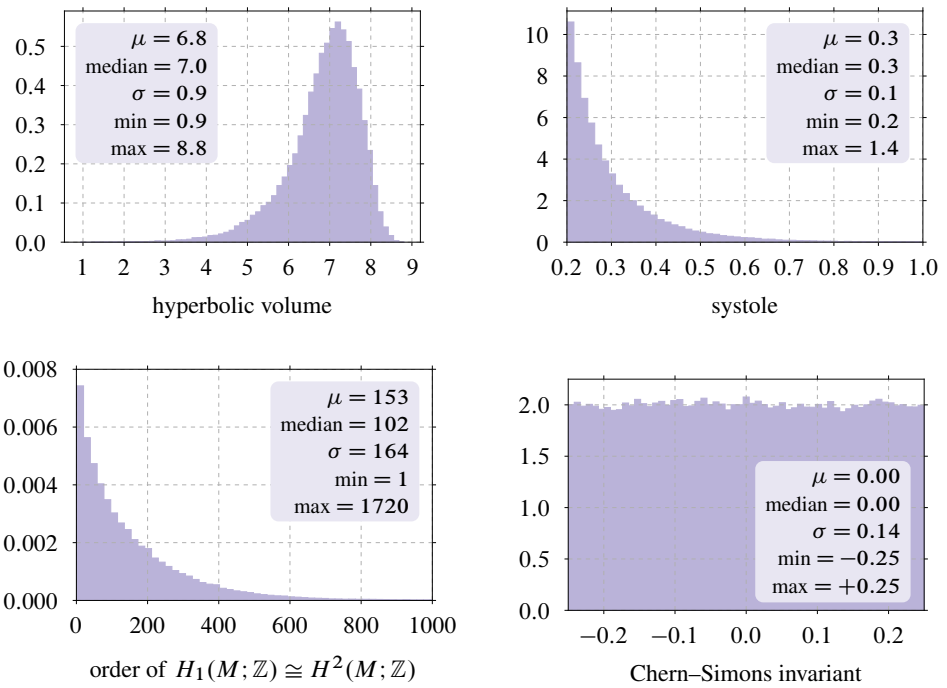

Figure 3: Some basic geometric and topological statistics about the manifolds in $\mathcal{Y}$ given as histograms. For similar plots about $\mathcal{C}$, see [23].

3 Details on the sample

3.1 Some rational homology solid tori

Burton proved there are precisely 61 911 cusped finite-volume hyperbolic 3–manifolds that have ideal triangulations with at most 9 tetrahedra [12]. Here, the equivalence is up to your choice of homeomorphism, diffeomorphism, or isometry, provided orientation-reversing maps are allowed. Each such manifold is the interior of a compact manifold whose boundary is a nonempty union of tori. Of these compact manifolds, some 59 068 (95.4%) are $\mathbb{Q}$–homology solid tori, and I will denote this collection of manifolds as $\mathcal{C}$.

3.2 The sample of rational homology spheres

The manifolds in $\mathcal{Y}$ in Theorem 1.6 are certain $\mathbb{Q}$–homology 3–spheres that are Dehn fillings on $\mathcal{C}$. While I conjecture that they are precisely the Dehn fillings on $\mathcal{C}$ that give hyperbolic $\mathbb{Q}$–homology spheres whose systole is at least 0.2, here I only establish

the weaker Theorem 1.4 that they are all hyperbolic and distinct. (A complete list of all nonhyperbolic fillings on $\mathcal{C}$ is known; see [23].) Some basic statistics about the manifolds of $\mathcal{Y}$ are shown in Figure 3, and I now turn to the proof of Theorem 1.4.

Proof of Theorem 1.4 To prove each manifold in $\mathcal{Y}$ is hyperbolic, I used the method of [47], as reimplemented by Goerner in [20]; see Section 6.1 of this paper for an overview of this technique. For this, as in the proof of Theorem 5.2 of [47], it was sometimes necessary to search around for a triangulation that could be used to certify the existence of a hyperbolic structure.

To prove that the manifolds of $\mathcal{Y}$ are distinct, I looked at finite quotients of their fundamental groups. Specifically, for $Y \in \mathcal{Y}$, consider $G = \pi_1(M)$. For a subgroup $H \leq G$ of finite index, associate the tuple

$$([G : H],\ [G : N],\ H^{\mathrm{ab}},\ N^{\mathrm{ab}}),$$

where $N = \mathrm{Core}(H)$ is the largest normal subgroup of G contained in H, and H^{ab} is the abelianization of H. The set of such tuples associated to subgroups of index at most n is an invariant of G and hence of Y. I used coset enumeration [49, Chapter 5] to compute this invariant for $n = 6$, which sufficed to distinguish all but 408 pairs of the manifolds in $\mathcal{Y}$. Those remaining pairs were separated by looking at the corresponding invariant for all $H \triangleleft G$ where G/H is simple and $[G : H] < 10\,000$. All of these group-theoretic calculations were done with Magma [4]. □

3.3 Remark The above proof of distinctness implies that all manifolds in $\mathcal{Y}$ have distinct profinite completions, which is an important open question for hyperbolic 3–manifolds generally; see [1, Question 1]. Also, Gardam [32] used a similar approach to the above to distinguish various census manifolds, including the 10 903 manifolds in $\mathcal{Y}$ from the original Hodgson–Weeks census. One difference from [32] is that I looked at the abelianization of the core (N^{ab}), as well as that of the subgroup itself (H^{ab}), allowing me to use H of smaller index than [32]. The expensive part of this technique is finding the subgroups H rather than computing their homology, and, as taking the core is cheap, including N^{ab} provides a major speedup.

3.4 Remark For finite-volume hyperbolic 3–manifolds with cusps, one can rigorously compute the canonical Epstein–Penner decomposition and use that to prove that two manifolds are *not* isometric [26]. However, for closed manifolds, to rigorously implement the procedure of [46] one needs to provably find and drill out the shortest closed geodesic, thus reducing the problem to the cusped case. An important open

question is whether one can use the certified hyperbolic structure produced via [47] to produce a provably correct shortest geodesic; see [75] for some work in this direction.

4 Finding the L–spaces

The simplest Heegaard Floer homology group $\widehat{\mathrm{HF}}$ is algorithmically computable by [68] and hence the property of being an L–space is algorithmically decidable. Moreover, the bordered Heegaard Floer theory of [57; 56] provides powerful and effective computational tools for computing $\widehat{\mathrm{HF}}$. This theory has been implemented in eg [79] and has been successfully applied to manifolds of the complexity of those in $\mathcal{Y}$, though one must first find a Heegaard splitting of the input manifold specified in terms of certain preferred generators of the mapping class group. However, rather than attack the problem of computing $\widehat{\mathrm{HF}}$ head on, I chose to use a bootstrapping procedure that exploited the structure of the big Dehn surgery graph [48] via the results of Rasmussen and Rasmussen [64] on L–space Dehn fillings. Throughout this section, complete code and manifold lists are available at [24].

4.1 Floer simple manifolds

So that I can explain my procedure, I first outline some results from [64]. Let M be a compact 3–manifold with ∂M a torus, and recall from Section 2 that $Sl(M)$ is the set of slopes on ∂M. Since we are interested in which Dehn fillings are L–spaces, define

$$\mathcal{L}(M) = \{\alpha \in Sl(M) \mid M(\alpha) \text{ is an L–space}\}.$$

Such an M is called *Floer simple* when it has *two* distinct Dehn fillings that are L–spaces, ie $|\mathcal{L}(M)| > 1$; see [64, Proposition 1.3]. For Floer simple manifolds, the set $\mathcal{L}(M)$ has the following structure; here, the Tureav torsion of M is a power series $\tau(M) \in \mathbb{Z}[\![t]\!]$ which is only slightly more complicated than the Alexander polynomial to compute.

4.2 Theorem [64, Theorem 1.6] *Suppose that M is a 3–manifold with ∂M a torus. If M is Floer simple, then $\mathcal{L}(M)$ is either a closed interval or consists of every slope except the homological longitude. If $\alpha \neq \beta$ are two known slopes in $\mathcal{L}(M)$, then $\mathcal{L}(M)$ can be explicitly computed from α, β, and the Turaev torsion of M.*

I leveraged this result to determine the L–spaces in $\mathcal{Y}$ by identifying a large number of manifolds in $\mathcal{C}$ as either Floer simple or not Floer simple. This was done by an inductive bootstrapping procedure that increased the level of knowledge about $\mathcal{Y}$ and $\mathcal{C}$

in tandem. I will describe this in detail below, but first I will explain the starting point with regards to which manifolds in $\mathcal{C}$ are Floer simple.

4.3 Priming the pump

Define M to be *Turaev simple* when every coefficient of $\tau(M) \in \mathbb{Z}[\![t]\!]$ is either 0 or 1. A basic obstruction to being Floer simple is:

4.4 Proposition [64, Proposition 1.4] *A Floer simple manifold M is Turaev simple.*

Computing $\tau(M)$ for all the manifolds in $\mathcal{C}$ identified 7895 of them as not Turaev simple and hence not Floer simple. To identify some initial Floer simple manifolds, I looked at *finite Dehn fillings*, that is, slopes α where $\pi_1(M(\alpha))$ is finite. Since any 3–manifold with finite fundamental group is an L–space, such an α is in $\mathcal{L}(M)$. An immediate consequence of the data in Theorem 1.2 of [23] is thus:

4.5 Corollary *There are exactly 59 200 finite Dehn fillings on manifolds in $\mathcal{C}$, with 78.2% having at least one such filling. There are 11 594 manifolds in $\mathcal{C}$ with two or more finite fillings, all of which are therefore Floer simple.*

4.6 Bootstrapping procedure

For 59.0% of the manifolds in $\mathcal{Y}$, I am aware of only a single description as a Dehn filling on something in $\mathcal{C}$. However, the remaining 41.0% average 3.4 known descriptions, and this will be the key to my procedure for expanding what we know about $\mathcal{Y}$ and $\mathcal{C}$ in tandem. The scheme is based on the following allowed deductions, where here "M is Floer simple" really means "M is Floer simple with at least two elements in $\mathcal{L}(M)$ explicitly known":

(D1) If $M \in \mathcal{C}$ has two Dehn fillings that are L–spaces, then M is Floer simple. (This is just the definition.)

(D2) If $M \in \mathcal{C}$ is Floer simple, then Theorem 4.2 determines exactly which of its Dehn fillings in $\mathcal{Y}$ are L–spaces.

(D3) If $M \in \mathcal{C}$ is not Floer simple and we know $M(\alpha)$ is an L–space, then every other manifold in $\mathcal{Y}$ which is a Dehn filling on M is not an L–space. (This is also just the definition.)

Table 1 shows what happens when using these three deductions starting from the data in Section 4.3; after repeated applications, one arrives at the "initial fixed point" where only 7.4% of the manifolds in $\mathcal{Y}$ have unknown L–space status.

$\mathcal{Y}$: $\mathbb{Q}$–hom. 3–spheres			$\mathcal{C}$: $\mathbb{Q}$–hom. solid tori			
L–sp	non-L	L–sp?	F-simp	non-F	simp?	
0	0	100	0	0	100	initial state
0	0	100	0	13.4	86.6	Proposition 4.4
0	24.3	75.7	0	13.4	86.6	(D3) with Corollary 4.5
0	24.3	75.7	19.6	13.4	67.0	(D1) with Corollary 4.5
7.7	26.1	66.2	19.6	13.4	67.0	$\mathcal{Y} \Leftarrow \mathcal{C}$ via (D2) and (D3)
7.7	26.1	66.2	45.0	13.4	41.7	$\mathcal{Y} \Rightarrow \mathcal{C}$ via (D1)
40.1	40.2	19.7	45.0	13.4	41.7	$\mathcal{Y} \Leftarrow \mathcal{C}$ via (D2) and (D3)
40.1	40.2	19.7	51.1	13.4	35.5	$\mathcal{Y} \Rightarrow \mathcal{C}$ via (D1)
46.8	45.6	7.6	51.1	13.4	35.5	$\mathcal{Y} \Leftarrow \mathcal{C}$ via (D2) and (D3)
46.9	45.8	7.4	51.2	13.4	35.4	initial fixed point
46.9	46.6	6.5	51.2	13.7	35.1	fixed point of (D1)–(D6)
47.0	46.6	6.4	85.7	13.7	0.6	(D1) and (D2) with Theorem 4.8
47.0	50.9	2.1	85.7	13.8	0.5	fixed point of (D1)–(D6)
47.0	53.0	0.001	85.7	14.1	0.2	foliations
47.0	53.0	0	85.7	14.1	0.2	last trick and final answer

Table 1: This table illustrates the steps in the proof of Theorem 1.6(1). The first three columns record the percentages of the manifolds of $\mathcal{Y}$ that are known to be L–spaces, known not to be L–spaces, and whose L–space status is unknown, respectively. The next three columns similarly record what is known about the manifolds in $\mathcal{C}$ being Floer simple. At the beginning, we are completely ignorant about which manifolds in $\mathcal{Y}$ are L–spaces and which manifolds in $\mathcal{C}$ are Floer simple. Then we apply the tools indicated in the rightmost column to learn more and more about both collections of manifolds. It takes five applications of each of (D1), (D2), and (D3) before the data stabilizes and becomes self-consistent, arriving at the row labeled "initial fixed point"; only the first three applications are shown individually as the others are indistinguishable at the level of rounding used in this table.

I now describe some more sophisticated deductions, for which I need to say a little more about [64]; for each Tureav simple M, the authors define from $\tau(M)$ a subset $\iota^{-1}(\mathcal{D}^{\tau}_{>0}(M))$ in $Sl(M)$ which is either empty or infinite with a single limit point, namely the homological longitude λ. The precise statement of [64, Theorem 1.6] is as follows. For a Floer simple M, if $\iota^{-1}(\mathcal{D}^{\tau}_{>0}(M))$ is empty, then $\mathcal{L}(M) = Sl(M) \setminus \{\lambda\}$; otherwise, if $\alpha \neq \beta$ are in $\mathcal{L}(M)$, then $\mathcal{L}(M)$ is the unique closed interval with

consecutive endpoints in $\iota^{-1}(\mathcal{D}^\tau_{>0}(M))$ containing both α and β. This allows for the following additional deductions when M is Turaev simple but may or may not be Floer simple:

(D4) If $\iota^{-1}(\mathcal{D}^\tau_{>0}(M))$ is empty and M has a non-L–space filling then M is not Floer simple.

(D5) If $\iota^{-1}(\mathcal{D}^\tau_{>0}(M))$ is nonempty and $\alpha \in \mathcal{L}(M)$, should M be Floer simple there are only one or two possibilities for $\mathcal{L}(M)$; there is one when α is not in $\iota^{-1}(\mathcal{D}^\tau_{>0}(M))$ and two when it is. If all possibilities for $\mathcal{L}(M)$ contain a known non-L–space filling, then we can conclude M is not Floer simple.

(D6) As in (D5), suppose $\iota^{-1}(\mathcal{D}^\tau_{>0}(M))$ is nonempty and $\alpha \in \mathcal{L}(M)$. As in (D5), should M be Floer simple there are at most two possibilities P_i for $\mathcal{L}(M)$. If a P_i contains a known non-L–space slope, it can be eliminated. Then any $\beta \in Sl(M)$ not in the union of the remaining P_i must be a non-L–space slope, even though we don't know whether or not M is Floer simple.

Applying all six deductions reduces the number of $\mathcal{Y}$ with unknown L–space status from 7.4% to 6.5%; see Table 1.

4.7 Endgame

From [23], we know there are exactly 201 798 exceptional Dehn fillings on manifolds in $\mathcal{C}$ which are $\mathbb{Q}$–homology 3–spheres, and so far I have only used the 59 200 that give spherical manifolds. One moreover has:

4.8 Theorem *Of the* 199 662 *exceptional $\mathbb{Q}$–homology sphere Dehn fillings on $\mathcal{C}$ that do not have a hyperbolic piece in their JSJ decompositions, exactly* 181 317 *are L–spaces and* 18 345 *are not.*

Proof As per Table 2 and Section 4.5 of [23], the 201 798 exceptional $\mathbb{Q}$–homology sphere fillings consist of 59 200 spherical manifolds, 4296 connected sums of spherical manifolds, 72 841 Seifert fibered manifolds with infinite π_1, 63 325 proper graph manifolds, and 2136 manifolds with a nontrivial JSJ decomposition with a hyperbolic piece. All spherical manifolds are L–spaces as are their connected sums since the connected sum of two L–spaces is again an L–space. For everything except the ones with a hyperbolic piece, it is possible to compute $\widehat{\mathrm{HF}}$ directly as follows. For each manifold, I translated from Regina's [13] description of the graph manifold given

in [23] over to the weighted tree description of [61]. In that form, I used Hanselman's program [41] associated to [40] to compute $\widehat{\mathrm{HF}}$. □

Beyond the spherical fillings which I already used, Theorem 4.8 provides an additional 140 462 fillings on $\mathcal{C}$ whose L–space status is known. Some 67 612 of these are fillings on manifolds in $\mathcal{C}$ that are already known to be Floer simple, so only 72 850 of these fillings provide new information, though the cases where we have two ways of determining whether an exceptional Dehn filling is an L–space give a strong check on the correctness of the computation. Combining Theorem 4.8 with repeated applications of the six deductions results in only 6437 (2.1%) of the manifolds in $\mathcal{Y}$ having unknown L–space status. It will turn out that only 3 are L–spaces and the other 6434 are non-L–spaces.

By Theorem 1.6(2), some 162 341 of the manifolds in $\mathcal{Y}$ have taut foliations and hence are not L–spaces; using this takes care of all but 3 of the manifolds in $\mathcal{Y}$. Moreover, the 8115 persistent foliar orientations of Theorem 8.6 tell us that 172 additional manifolds in $\mathcal{C}$ are not Floer simple.

The three remaining manifolds in $\mathcal{Y}$ are all Dehn fillings on $o9_{34146}$, which is Turaev simple and has a single known L–space filling, namely $o9_{34146}(1,0)$, which is the lens space $L(35,11)$. I claim that $o9_{34146}(0,1)$ is also an L–space; in this case, the manifold $o9_{34146}$ is then Floer simple and we can finish off the last three manifolds in $\mathcal{Y}$. The filling $o9_{34146}(0,1)$ is hyperbolic but it is not in $\mathcal{Y}$ because its systole is ≈ 0.08648 which is less than 0.2. SnapPy confirms that $o9_{34146}(0,1)$ is homeomorphic to $m007(11,3)$. Now $m007$ is already known to be Floer simple and using (D2) gives that $m007(11,3) = o9_{34146}(0,1)$ is an L–space. This completes the proof of Theorem 1.6(1). For code and further details see [24].

4.9 Remark In the end, we know at least 50 598 (85.7%) of the manifolds in $\mathcal{C}$ are Floer simple and at least 8352 (14.1%) are not Floer simple but there are 118 (0.2%) whose status is unknown. The first ten unknown ones are $t08191$, $t08263$, $o9_{10045}$, $o9_{18999}$, $o9_{19314}$, $o9_{19325}$, $o9_{19344}$, $o9_{19372}$, $o9_{19424}$, and $o9_{19478}$.

5 Proving groups are not orderable

This section is devoted to proving Theorem 1.6(4), which is restated here:

5.1 Theorem *At least* 110 940 *of the manifolds in* $\mathcal{Y}$ *are not orderable.*

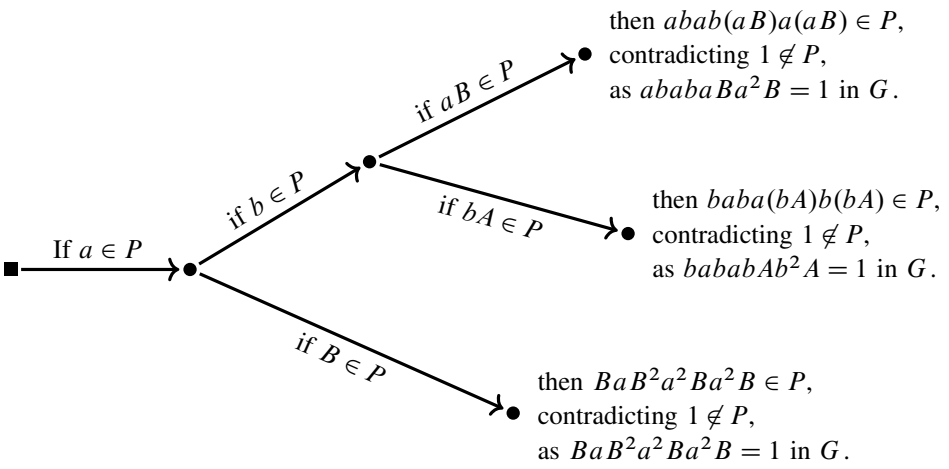

Figure 4: This figure illustrates the proof of Theorem 9.1 of [16], namely that the group $G = \langle a, b \mid ababaBa^2B, ababAb^2Ab\rangle$ is not left-orderable; here $A = a^{-1}$ and $B = b^{-1}$. (The group G is the fundamental group of the Weeks manifold.) The nonordering tree should be read starting from the leftmost vertex and encodes a proof by contradiction: we assume that a positive cone P exists, and then consider all possibilities for whether certain nontrivial elements of G are or are not in P. In each case, the contradiction comes from showing that $P \cdot P \subset P$ implies that $1 \in P$. Because we can reverse the roles of P and P^{-1}, we need not consider the case when $A \in P$.

The basic approach follows [16, Sections 8–10], with the most significant change being how the word problem is solved in the relevant 3–manifold groups. This is discussed in Section 6 below and is the key for going from proving 44 manifolds are not orderable in [16] to more than 100 000 manifolds here. The precise list of the manifolds in Theorem 5.1 is available at [24] along with the code and additional data needed to prove it.

5.2 Proof trees

For Theorem 5.1, each manifold in the statement was handled separately, though in a uniform manner as I will now describe. Specifically, for each one I found a proof of nonorderability that has a structure implicit in many arguments that a group is not left-orderable, including those in [16]. To formalize this kind of proof, I first need to fix the general context. Let G be a group with a fixed finite generating set S. Suppose further we have a solution to the word problem for G, that is, an algorithm that determines whether or not a word in S corresponds to the trivial element in G. If we have a left order

on G, we consider its *positive cone* $P = \{g \in G \mid g > 1\}$. This gives a partition of G into $P \cup P^{-1} \cup \{1\}$ such that $P \cdot P \subset P$. (Conversely, any such P gives an associated order [18, Section 1.4].) The prototype proof of nonorderability is given in Figure 4, and the following formal definition is most easily understood in the context of that example.

5.3 Definition A *nonordering tree* for a group G with generators S is a finite trivalent tree T with the following additional structure:

(1) The tree T has a preferred root vertex, and all edges of T are oriented pointing away from this root.

(2) Each edge of T is labeled by an element of $\mathrm{FreeGroup}(S)$. At each interior vertex of T, the labels on the two outgoing edges are inverses in $\mathrm{FreeGroup}(S)$.

(3) Each leaf vertex, other than the root, is labeled by a word in the edge labels that appear along the unique directed path from the root to the leaf.

(4) Every edge label corresponds to a nontrivial element of G, but every leaf label corresponds to 1 in G.

Note that a nonordering tree is a finite combinatorial object, and that if we can solve the word problem in G then we can check whether a given labeled tree satisfies (1)–(4). It is straightforward to generalize the thinking behind the example in Figure 4 to show:

5.4 Theorem *Suppose G has a nonordering tree T. Then G is not left-orderable.*

The converse to Theorem 5.4 turns out to be true as well, but I have no use for this fact here. I will now outline the proof of Theorem 5.1.

Proof of Theorem 5.1 For each of the manifolds in the statement, I used a heuristic method (described in Section 5.5 below) to find a likely nonordering tree for its fundamental group. I then certified that each labeled tree was in fact a nonordering tree using the solution to the word problem given in Section 6. The largest tree was for the manifold $o9_{39416}(4,1)$, which had some 20 329 leaves and 40 655 edges, though the median nonordering tree had only 12 leaves and 21 edges. In total, there were 17.1 million instances of the word problem to solve and the longest word considered had length 76 196. You can find the labeled tree for each manifold at [24], along with the code used to verify them. All together, the labeled trees weigh in at some 919MB of data, making this one very long proof. □

5.5 Finding nonordering trees

To find a nonordering tree for each manifold, I used the procedure described in [16, Section 8], but using a fast, although nonrigorous, method to "solve" the word problem. Specifically, for a given $G = \pi_1(Y)$ with $Y \in \mathcal{Y}$, I used SnapPy [20] to find the images of a generating set S of G under an alleged holonomy representation $\rho\colon \pi_1(Y) \to \mathrm{SL}_2\mathbb{C}$ as matrices with double-precision floating-point entries. To test if a word in S is 1 in G, I multiplied the corresponding matrices and checked if the result was close to the identity matrix in $\mathrm{SL}_2\mathbb{C}$. While errors can and do accumulate in this situation [28], the words in question typically had length less than 10, and the fact that we're approximating a *discrete* subgroup in $\mathrm{SL}_2\mathbb{C}$ makes this quite numerically robust in practice. Indeed, not a single one of the 110 940 proofs found this way turned out to be incorrect when it was rigorously verified using the solution to the word problem of Section 6. I am grateful to Saul Schleimer for suggesting attacking the word problem in this way, rather than the original approach in [16], which used the theory of automatic groups.

The procedure of [16, Section 8] is to look at a ball B_r of radius r in the Cayley graph of G with respect S, and try to partition B_r into $P \cup P^{-1} \cup \{1\}$ so that P is closed under multiplications that stay in B_r. (To give a sense of scale, for most manifolds in Theorem 5.1, I looked at a B_r with 5000 to 30 000 elements.) Because G has exponential growth, exactly which elements are in B_r is very sensitive to the choice of generating set S, even if we choose r so that the number of elements in B_r is roughly constant. One obvious choice, and the one used in [16, Section 10], is to minimize the size of S. However, I got much better results (that is, found more nonordering trees) starting with presentations that had more than the minimal number of generators but relatively short relators. A typical example is this presentation for $\pi_1(o9_{36382}(5,1))$:

$$\langle a, b, c, d, e, f \mid bdbbd,\ adBf,\ cAefB, adFcACd,\ deeC,\ aaaaaBcc\rangle.$$

5.6 Remark In searching for the proofs that formed Theorem 5.1, I always used the default Dehn surgery description of Y and group presentation produced by SnapPy with the option `minimize_number_of_generators=False`. Working with a greater variety of descriptions and presentations would certainly show that several thousand additional manifolds are nonorderable. For example, the very simple L–spaces $m006(3,1)$ and $m016(6,1)$ are not listed as nonorderable in [24], though in fact both are. The first is excluded because the technique of Section 6.1 does not apply to

this description (some shape z has $\operatorname{Im} z < 0$), but this can be fixed by using the description $m011(3,1)$. The second example can easily be handled by switching to the description $s002(-3,2)$ for whatever reason.

6 Solving the word problem

Studying hyperbolic structures on 3–manifolds numerically has a history that goes back 40 years to Riley [66], with much work being done using Thurston's perspective of ideal triangulations and gluing equations (see [73; 78]) via the program SnapPea and its successors [20]. While these methods provide robust and compelling numerical evidence for the existence and particulars of a hyperbolic structure for many a 3–manifold, they do not prove that a given manifold is hyperbolic much less guarantee that any hyperbolic invariants computed (eg the volume) are approximately correct. However, the breakthrough paper [47] shows how many of these numerical computations can be made fully rigorous with remarkably few changes using the framework of interval arithmetic and interval analysis. I now recall their method and explain how to use it to rigorously solve the word problem for the fundamental group of a given finite-volume hyperbolic 3–manifold. While there are several other ways to solve the word problem here, for example using the Knuth–Bendix procedure to find and certify a short-lex automatic structure [27], the present approach is by far the most efficient I know of and the only one fast enough for proving Theorem 5.1.

6.1 Interval analysis

In interval analysis, a number $z \in \mathbb{C}$ is partially specified by giving a closed rectangle $\boldsymbol{z}$ with vertices in $\mathbb{Q}(i)$ that contains z. Because the vertices are rational, such intervals can be exactly stored on a computer and rigorously combined by the operations $+$, $-$, $\times$ and $/$ to create other such intervals; see eg [59; 67] for general background on interval analysis and its applications. One cost is that the sizes of the rectangles grow with the number of operations. I will use $\mathrm{I}\mathbb{C}$ to denote the set of such complex intervals. Two elements of $\mathrm{I}\mathbb{C}$ are not viewed as equal even when all their vertices agree since each represents some unknown point inside the rectangle. In contrast, when two elements of $\mathrm{I}\mathbb{C}$ are disjoint they are considered not equal.

The key tools of interval analysis needed here are effective versions of the inverse function theorem. For a suitable smooth function $f\colon \mathbb{C}^n \to \mathbb{C}^n$ these results provide simple tests for proving that f has a zero in some interval vector $\boldsymbol{z} \in \mathrm{I}\mathbb{C}^n$. Suppose Y

is a closed 3–manifold specified by Dehn fillings on a topological ideal triangulation $\mathcal{T}$. If $\mathcal{T}$ has n tetrahedra, the logarithmic form of Thurston's gluing equations gives a smooth map $f\colon \mathbb{C}^n \to \mathbb{C}^n$ where a zero z of f gives a hyperbolic structure on Y provided the imaginary parts of all z_i are positive; here each z_i specifies the geometric shape in $\mathbb{H}^3$ of one of the tetrahedra in $\mathcal{T}$. In favorable circumstances, one can apply the interval Newton's method or Krawczyk's test to prove that an interval vector $\boldsymbol{z} \in \mathrm{I}\mathbb{C}^n$ contains a zero of f of the needed type. In this case, the hyperbolic structure on Y is known in terms of the shapes of the tetrahedra of $\mathcal{T}$ to within a tolerance determined by the sizes of the rectangles $\boldsymbol{z}_i$. A $\boldsymbol{z} \in \mathrm{I}\mathbb{C}^n$ that has been proven to contain such a zero of f will be called an *approximate hyperbolic structure*. The authors of [47] demonstrated this approach works fantastically well in practice, in particular certifying the existence of hyperbolic structures on more than 27 000 manifolds.

For the computations here, I used Goerner's implementation of this approach included in SnapPy [20] when used inside SageMath [72]. The original code of [47] used elements of $\mathrm{I}\mathbb{C}$ whose vertices are machine precision floating point numbers. This provides maximum speed but limits how small one can make the rectangles $\boldsymbol{z}_i$ in an approximate hyperbolic structure; in contrast, SnapPy allows arbitrary precision vertices. While this is significantly slower, for the manifolds here it still takes less than a second to use the interval Newton's method to certify an approximate hyperbolic structure where each $\boldsymbol{z}_i$ has diameter less than 10^{-1000}. Using the interval implementation of the dilogarithm function provided by Arb [51], such an approximate hyperbolic structure allows SnapPy to give the volume of one of these manifolds to 1000 provably correct digits, though it takes an additional 5–10 seconds to do so.

6.2 Approximate holonomy representations

Let $M_2(\mathrm{I}\mathbb{C})$ denote 2-by-2 matrices with entries in $\mathrm{I}\mathbb{C}$. The arithmetic operations on $\mathrm{I}\mathbb{C}$ naturally give addition and multiplication operations on $M_2(\mathrm{I}\mathbb{C})$. Let $\mathrm{GL}_2(\mathrm{I}\mathbb{C})$ be the elements of $M_2(\mathrm{I}\mathbb{C})$ whose determinant, itself an element of $\mathrm{I}\mathbb{C}$, does not contain 0. While many products of elements of $\mathrm{GL}_2(\mathrm{I}\mathbb{C})$ are again in $\mathrm{GL}_2(\mathrm{I}\mathbb{C})$, it is not actually closed under multiplication. Suppose G is the fundamental group of a hyperbolic 3–manifold Y with a finite symmetric generating set S. Any holonomy representation from G to $\mathrm{Isom}^+(\mathbb{H}^3) = \mathrm{PSL}_2\mathbb{C}$ of the hyperbolic structure on Y lifts to a representation $G \to \mathrm{SL}_2\mathbb{C}$ which I will still call a holonomy representation. An *approximate holonomy representation* is a function $\boldsymbol{\rho}\colon S \to \mathrm{GL}_2(\mathrm{I}\mathbb{C})$ such that there is a holonomy representation $\rho_0\colon G \to \mathrm{SL}_2\mathbb{C}$ so that $\rho_0(\gamma) \in \boldsymbol{\rho}(\gamma)$ for all $\gamma \in S$.

Given a word $w = s_1 s_2 \cdots s_n$ in S, define $\boldsymbol{\rho}(w) = \rho(s_1)\rho(s_2)\cdots\rho(s_n)$, as you would expect. Regardless of whether $\boldsymbol{\rho}(w)$ is in $\mathrm{GL}_2(\mathrm{I}\mathbb{C})$ or just $M_2(\mathrm{I}\mathbb{C})$, we are guaranteed that $\rho_0(w) \in \boldsymbol{\rho}(w)$.

In the setup of Section 6.1, suppose a finite-volume hyperbolic 3–manifold Y is specified by an approximate hyperbolic structure $\boldsymbol{z}$ on an ideal triangulation $\mathcal{T}$. Since we know the approximate shapes of the geometric ideal tetrahedra in $\mathcal{T}$, we can start tiling out to build an approximation of the developing map between the universal cover of $\mathcal{T}$ and $\mathbb{H}^3$ and use that to compute an approximate holonomy representation; see eg [25, Lemma 3.5] for details.

6.3 Solving the word problem

Suppose w is a word in our generators S of $G = \pi_1(Y)$ and we wish to know if $w = 1$ in G. If $\boldsymbol{\rho}$ is an approximate holonomy representation and $\boldsymbol{\rho}(w)$ does not contain the identity matrix I, then we have proved that $w \neq 1$ in G since then there is an actual holonomy representation ρ_0 with $\rho_0(w) \neq I$. However, if instead $I \in \boldsymbol{\rho}(w)$, we cannot immediately conclude $w = 1$ since $\boldsymbol{\rho}(w)$ might contain other elements of $\rho_0(G)$ as well. Fortunately, the subgroup $\rho_0(G)$ is discrete in $\mathrm{SL}_2\mathbb{C}$, so if the entries of $\boldsymbol{\rho}(w)$ have small enough diameter then $I \in \boldsymbol{\rho}(w)$ does imply $\rho_0(w) = I$ and hence $w = 1$. This can be made effective by exploiting Jørgensen's inequality:

6.4 Theorem *Suppose $\boldsymbol{\rho}$ is an approximate holonomy representation for a hyperbolic 3–manifold Y where s_1 and s_2 are in S with $2 \notin \mathrm{tr}(\boldsymbol{\rho}([s_1, s_2]))$. If w is a word in S with*

$$|\mathrm{tr}^2(\boldsymbol{\rho}(w)) - 4| + |\mathrm{tr}([\boldsymbol{\rho}(s_i), \boldsymbol{\rho}(w)]) - 2| < 1 \tag{6.5}$$

for each $i = 1, 2$, then $w = 1$ in $G = \pi_1(Y)$.

Here, the left-hand side of (6.5) is a real interval and the equation should be read as saying both of its endpoints are less than 1.

Proof of Theorem 6.4 Let ρ_0 be a holonomy representation compatible with $\boldsymbol{\rho}$. For this proof, we will focus on the action of elements of G on $\mathbb{H}^3$, and so regard ρ_0 as a representation $G \to \mathrm{PSL}_2\mathbb{C}$. By hypothesis, we have $\rho_0([s_1, s_2]) \neq I$ and so neither $\rho_0(s_i)$ is equal to I and moreover $\langle \rho_0(s_1), \rho_0(s_2) \rangle$ is a nonelementary torsion-free discrete subgroup of $\mathrm{PSL}_2\mathbb{C}$.

For each i, equation (6.5) implies that Jørgensen's inequality (see eg [58, Theorem 2.17]) is violated for the pair $\rho_0(w)$ and $\rho_0(s_i)$; in particular, $\Gamma_i = \langle \rho_0(w), \rho_0(s_i) \rangle$ cannot be a nonelementary discrete subgroup of $\mathrm{PSL}_2\mathbb{C}$. Since Γ_i is discrete, this means it must be elementary. By eg [58, Proposition 2.2], as Γ_i is torsion-free the nontrivial elements of Γ_i are either all parabolic with a common fixed point on $\partial\mathbb{H}^3$ or all hyperbolic with a common axis in $\mathbb{H}^3$. So if $\rho_0(w) \neq I$, then $\langle \rho_0(s_1), \rho_0(s_2) \rangle$ would also be elementary, a contradiction. So $\rho_0(w) = I$ and hence $w = 1$ in G as needed. □

6.6 Practical considerations

Any given approximate holonomy representation $\boldsymbol{\rho}$ will not solve the word problem for all w as the intervals making up $\boldsymbol{\rho}(w)$ frequently "smear out" to the point where $I \in \boldsymbol{\rho}(w)$ but Theorem 6.4 does not apply. Thus to determine whether a given w is equal to 1 in G, you may need to refine the approximate hyperbolic structure to get one accurate enough so that the associated $\boldsymbol{\rho}$ can determine whether $\rho_0(w) = 1$ or not. In the proof of Theorem 5.1, for 78.0% of the manifolds it sufficed to use approximate hyperbolic structures that were correct to about 100 bits of precision (about 30 decimal digits, or roughly twice that of an IEEE-754 double-precision floating point number), though 22.0% of the manifolds needed 200 bits for some words, and 11 manifolds (0.01%) needed 400 bits. As mentioned above, the longest word w that was considered in Theorem 5.1 had length $|w| = 76\,196$, which makes these precision requirements seem modest by comparison. In fact, this particular w only required $\boldsymbol{\rho}$ to be computed to 200 bits, which resulted in the entries of the $\boldsymbol{\rho}(s)$ for $s \in S$ having diameter about 2^{-175}, whereas the entries of $\boldsymbol{\rho}(w)$ had diameter about 2^{-31}.

7 Foliar orientations

A *triangulation* of a closed 3–manifold is a cell complex made out of finitely many tetrahedra with all their 2–dimensional faces identified in pairs via affine maps so that the link of every vertex is a 2–sphere. (For such face gluings, the link condition is equivalent to the complex being a closed 3–manifold; see eg [74, Proposition 3.2.7].) In particular, a triangulation is not necessarily a simplicial complex, but rather what is sometimes called a semisimplicial triangulation or pseudotriangulation.

An *edge orientation* of a 3–manifold triangulation $\mathcal{T}$ is a choice of direction for each edge of the 1–skeleton $\mathcal{T}^1$. An edge orientation μ of $\mathcal{T}$ is *acyclic* when there is no face

of $\mathcal{T}^2$ where μ orients its edges as a directed cycle. Thus, in an acyclic edge orientation, each face of $\mathcal{T}$ has the orientation pattern shown in Figure 5, left, and the edges of the face are called *long* or *short* as indicated, with the short edges further subdivided into *bottom* and *top*. A simple case check shows that any acyclic edge orientation of a tetrahedron is as in Figure 5, right, up to a possibly orientation-reversing homeomorphism. (An acyclic edge orientation gives an ordering of the vertices of each simplex of $\mathcal{T}$ making it into a Δ–complex as defined in [43, Section 2.1], and indeed in our context these two notions are equivalent.) In each such tetrahedron, the unique edge that is long in both of its adjacent faces is called *very long*. The two edges labeled *compatibly short* are those that are the same kind of short edge in both of their adjacent faces.

Now suppose μ is an acyclic edge orientation of $\mathcal{T}$. First, an edge of $\mathcal{T}$ is a *sink edge* with respect to μ when it is very long in every tetrahedron for which it is adjacent. Second, the *face relation* of μ is the equivalence relation on the faces of $\mathcal{T}^2$ generated by the rule that for each compatibly short edge in a tetrahedron the two faces adjacent to it are equivalent. To visualize the equivalence classes of the face relation, consider the dual cellulation $\mathcal{D}$ to $\mathcal{T}$, where in particular the edges of $\mathcal{D}^1$ correspond to the faces of $\mathcal{T}^2$. In each tetrahedron σ of $\mathcal{T}$, slice $\mathcal{D}^1 \cap \sigma$ into two pieces at the vertex in $\mathcal{D}^0$ via a quadrilateral that separates the two compatibly short edges and is otherwise disjoint from $\mathcal{D}^1$. This cuts $\mathcal{D}^1$ into a collection of closed loops which correspond precisely to the equivalence classes of the face relation.

I now focus on the case when $\mathcal{T}$ has a single vertex. Putting these concepts together, a *foliar orientation* of $\mathcal{T}$ is an acyclic edge orientation that has no sink edges, and whose face relation has a single equivalence class. The key result of this section is:

7.1 Theorem *Suppose $\mathcal{T}$ is a 1–vertex triangulation of a closed orientable 3–manifold Y that admits a foliar orientation μ. Then Y has a coorientable taut foliation $\mathcal{F}$ that is transverse to $\mathcal{T}^1$ and induces the edge orientation μ.*

Having a foliar orientation is a strengthening of Calegari's notion of a local orientation for a 3–manifold triangulation [14]. Specifically, for a 1–vertex triangulation, it turns out that Calegari's local orientation condition is equivalent to an acyclic edge orientation whose face relation has a single equivalence class, and thus the added restriction is that there are no sink edges. The basic idea for Theorem 7.1 is to build a branched surface that is "dual" to the foliar orientation as shown in Figure 6, and then apply Li's foundational work on laminar branched surfaces [55] to prove the existence of a related foliation.

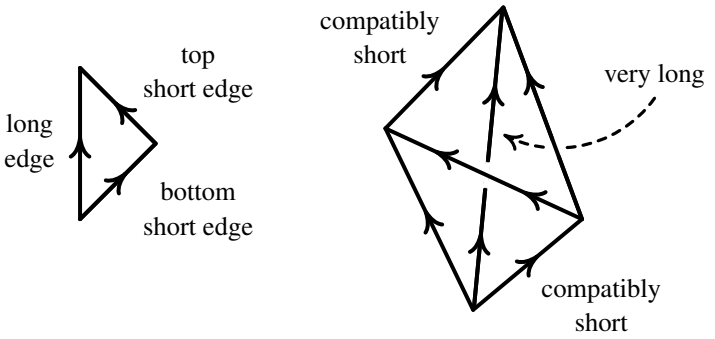

Figure 5: Local possibilities for acyclic edge orientations.

7.2 Branched surfaces

Figure 6 shows how to associate a branched surface $B(\mu)$ to any acyclic edge orientation μ; note here that μ gives a global coorientation to $B(\mu)$; since Y is orientable, this gives a global orientation to the branches of $B(\mu)$. The key property is that when μ is foliar then $B(\mu)$ is a laminar branched surface as defined by Li [55].

Proof of Theorem 7.1 Within this proof, I will use concepts and notation from [55, Sections 0–1] without further comment and also abbreviate $B(\mu)$ to B. To start, let us understand the topology of the guts $G = Y \setminus \mathrm{int}(N(B))$, where $N(B)$ is a regular

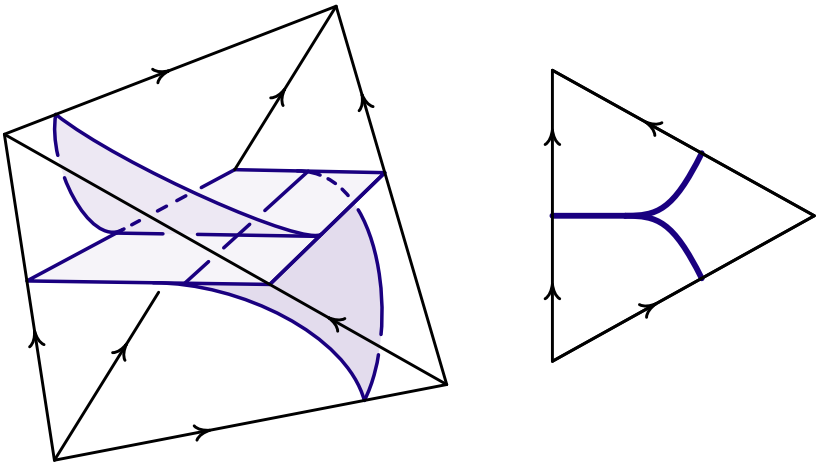

Figure 6: The branched surface $B(\mu)$ in one tetrahedron. Note that each face of the tetrahedron looks like the figure at right, and hence these local pictures glue up to give a branched surface in $\mathcal{T}$.

neighborhood of B. As $\mathcal{T}$ has a single vertex, we see from Figure 6 that G is a single 3–ball and to complete the picture we need to understand how the horizontal boundary $\partial_h N(B)$ and vertical boundary $\partial_v N(B)$ decompose the sphere ∂G. Each tetrahedron of $\mathcal{T}$ contributes two rectangles to $\partial_v N(B)$, and the gluing pattern of these rectangles matches the face relation of μ; since the face relation has a single equivalence class, the vertical boundary $\partial_v N(B)$ is a single annulus and so the horizontal boundary $\partial_h N(B)$ is two discs. Hence G is just a $D^2 \times I$ region.

I next show that B is laminar. As per Definition 1.4 of [55], there are four conditions to check. The first two conditions are (1) and (2) from Proposition 1.1 of [55], namely that $\partial_h N(B)$ is incompressible in G, that no component of $\partial_h N(B)$ is a sphere, that G is irreducible, and finally that G has no monogons; all of these are immediate since G is a $D^2 \times I$ region. The third condition is (3) of Proposition 1.1 of [55], namely that B does not carry a torus that bounds a solid torus in Y. To see this, first note that any surface S carried by B inherits an orientation from B and moreover S has strictly positive algebraic intersection number with each μ–oriented edge of $\mathcal{T}$ that it meets. Since $\mathcal{T}$ has one vertex, each edge is a closed loop, and so we conclude S is nonseparating and in particular does not bound a solid torus as required. The fourth and final condition to check is that, after collapsing all trivial bubbles, the branched surface B has no sink discs where all cusps point inward. As G is connected, there are no trivial bubbles; looking back at Figure 6, the only local branch that could contribute to a sink disk for B is the square that meets the very long edge. The hypothesis that $\mathcal{T}$ has no sink edges with respect to μ thus gives exactly that B has no sink discs. Therefore, we have shown that B is laminar.

Here is how to build the foliation promised in the theorem. By Theorem 1(a) of [55], as B is laminar it fully carries an essential lamination. Since the guts of B is a $D^2 \times I$ region, we can extend this lamination to a foliation $\mathcal{F}$ of Y that is transverse to $\mathcal{T}^1$ and induces the orientation μ there. The foliation $\mathcal{F}$ is taut since the edges of $\mathcal{T}$ form a collection of transverse closed loops meeting every leaf. □

7.3 Examples

Foliar orientations are extremely common in practice, and I was able to use them to prove 98.6% of Theorem 1.6(2):

7.4 Theorem *At least* 160 003 *of the manifolds in* $\mathcal{Y}$ *have* 1*–vertex triangulations admitting foliar orientations.*

The rest of Theorem 1.6(2) will be handled using a related technique introduced in Section 8. I will now outline the proof of Theorem 7.4.

Proof of Theorem 7.4 For each manifold Y in $\mathcal{Y}$, a variety of 1–vertex triangulations were generated by doing random Pachner moves starting from the manifold's various descriptions as Dehn fillings on manifolds in $\mathcal{C}$. For each such triangulation, an exhaustive search for foliar orientations was done using the method of Section 7.9. The first such triangulation found and all of its foliar orientations were saved and can be found at [24] together with the relevant code. The saved triangulations averaged 21.8 distinct foliar orientations each (modulo a complete reversal of signs); there were 1215 triangulations with a unique foliar orientation, and the largest number of foliar orientations for a single triangulation was 884. □

7.5 Triangulations with more vertices

Here is one way to generalize Theorem 7.1 to triangulations with more than one vertex. Throughout, let $\mathcal{T}$ be a triangulation of a closed orientable 3–manifold Y. First, an edge orientation μ of $\mathcal{T}$ is *strongly connected* when the directed graph $(\mathcal{T}^1, \mu)$ is strongly connected, ie every pair of vertices v_0 and v_1 in $\mathcal{T}^0$ are joined by a μ–directed path $\mathcal{T}^1$ that starts at v_0 and ends at v_1. Second, I will say that $\mathcal{T}$ has *short loops* if for every vertex v of $\mathcal{T}^0$ there is an edge in $\mathcal{T}^1$ which joins v to itself. Finally, an acyclic edge orientation μ of $\mathcal{T}$ is *foliar* when $\mathcal{T}$ has short loops and μ is strongly connected, has no sink edges, and where the number of equivalence classes of its face relation is equal to the size of $\mathcal{T}^0$. Note that when $\mathcal{T}$ has only one vertex this is equivalent to the original definition of foliar. Again, we have:

7.6 Theorem *Suppose $\mathcal{T}$ is a triangulation of a closed orientable 3–manifold Y that admits a foliar orientation μ. Then Y has a coorientable taut foliation $\mathcal{F}$ that is transverse to $\mathcal{T}^1$ and induces the edge orientation μ.*

Proof of Theorem 7.6 The proof is very similar to that of Theorem 7.1. Let $B = B(\mu)$ be the branched surface associated to μ. The condition on the face relation of μ means that the guts $Y \setminus \operatorname{int}(N(B))$ is a union of $D^2 \times I$ regions, one for each vertex of $\mathcal{T}$. Moreover, since $\mathcal{T}$ has short loops none of these are trivial bubbles, which means there is nothing to collapse before checking for sink disks, and B of course has none of these since μ lacks sink edges. Finally, as μ is strongly connected, the argument from before shows that B cannot carry a separating surface. Thus B is laminar and fully

carries an essential lamination, which we can again fill in to get a foliation $\mathcal{F}$ which will be taut since the needed family of transverse loops can be constructed using that μ is strongly connected. □

For the 3000 non-L–spaces that are not foliated by Theorem 7.4, I searched for 2–vertex triangulations to which Theorem 7.6 applied, without a great deal of success:

7.7 Theorem *There at least* 174 *manifolds in* $\mathcal{Y}$ *not covered by Theorem 7.4 with* 2*–vertex triangulations that admit a foliar orientation.*

As always, the specific manifolds and source code are at [24].

7.8 Remark I do not know if every coorientable taut foliation $\mathcal{F}$ of Y arises from a foliar orientation. Here are two approaches for trying to show this is the case:

(1) Blow some air into $\mathcal{F}$ to get an essential lamination of Y with nonempty complement, and then apply [55] to get a laminar branched surface B that carries it. The guts of B must be product regions, and if they are not $D^2 \times I$ then add some extra branches to B to cut them down into such regions. After collapsing any trivial bubbles, try to build a cell complex that is dual to B and modify it to one that is a triangulation.

(2) Alternatively, you could start with the kind of triangulation considered in [29] which is transverse to $\mathcal{F}$ and supports a combinatorial volume-preserving flow; these have some thematic similarities with foliar orientations.

Unfortunately, it seems unlikely that either approach would give an algorithm for determining whether Y has such a foliation, much less one that is actually implementable and practical.

7.9 Searching for foliar orientations

Since the Euler characteristic of a closed 3–manifold is 0, a 1–vertex triangulation $\mathcal{T}$ with n tetrahedra has $n+1$ edges. Fixing the orientation of the first edge arbitrarily, there are 2^n edge orientations to search through when looking for a foliar orientation. As I considered triangulations with a median of 19 and a maximum of 27 tetrahedra, this makes a completely naive search infeasible. I dealt with this by reframing the task as a boolean satisfiability (SAT) problem and used a general-purpose SAT solver to enumerate all acyclic edge orientations, from which the foliar ones were easily selected.

Although SAT is NP–complete and enumerating all solutions to a SAT problem is #P–complete, modern heuristic solvers make short work of problems of the size and type that arise here.

Here is the basic idea. Given a 1–vertex triangulation $\mathcal{T}$, arbitrarily fix some edge orientation μ_0. Any other edge orientation μ is then encoded by using one boolean variable per edge to record whether μ agrees with μ_0 there. For each face σ of $\mathcal{T}^2$ there is a boolean clause equivalent to the orientation being acyclic there as follows. Let ϵ_i, ϵ_j, and ϵ_k be the variables associated to the three edges of σ. If μ_0 orients $\partial\sigma$ as a cycle, then μ is acyclic if and only if

$$(\epsilon_i \vee \epsilon_j \vee \epsilon_k) \wedge (\neg\epsilon_i \vee \neg\epsilon_j \vee \neg\epsilon_k).$$

If μ_0 does not orient $\partial\sigma$ as a cycle, one can always create a cycle by reversing one of the edges and use this to formulate the correct clause. For example, if reversing the orientation on the edge associated to ϵ_i creates a cycle, then μ is acyclic if and only if

$$(\neg\epsilon_i \vee \epsilon_j \vee \epsilon_k) \wedge (\epsilon_i \vee \neg\epsilon_j \vee \neg\epsilon_k).$$

Thus finding all acyclic edge orientations is equivalent to finding all solutions to a certain SAT problem, specifically a 3–SAT problem with n variables and $4n$ clauses in conjunctive normal form.

I used CryptoMiniSat [71] for the enumeration. On a sample of about 2900 triangulations with 22 tetrahedra each, the average time to enumerate all acyclic edge orientations was 0.02 seconds per triangulation, and the largest number of acyclic edge orientations found was 1138, which is quite small compared to $2^{22} \approx 4.2$ million.

7.10 Remark The number of acyclic edge orientations can in fact be exponentially large in the size of $\mathcal{T}$, which precludes a universal polynomial-time algorithm for enumerating them. Here is one easy if somewhat degenerate way to see this. Start with any $\mathcal{T}$ that has an acyclic edge orientation μ. Pick any tetrahedron in $\mathcal{T}$ and do a $0 \to 2$ move on the pair of faces adjacent to its very long edge; that is, unglue those faces from their neighbors and insert a "pillow" consisting of two new tetrahedra that form the link of a new valence to edge τ. If $\mathcal{T}'$ is the new triangulation, then μ can be extended to $\mathcal{T}'$ by *either* orientation of τ. Repeating n times gives a triangulation with $2n + c$ tetrahedra and at least 2^n acyclic edge orientations.

8 Persistently foliar orientations

I now describe an analog of foliar orientations for a manifold with torus boundary which gives taut foliations on all but one of its Dehn fillings. The approach is motivated by the constructions of taut foliations on all nontrivial Dehn surgeries on certain knots in S^3; see Section 8.2 below. Specifically, let M be an orientable 3–manifold with ∂M a single torus. An *ideal triangulation* of M is a cell complex $\mathcal{T}$ obtained from finitely many tetrahedra by identifying their faces in pairs so that $\mathcal{T}^0$ is a single point whose complement is homeomorphic to $M \setminus \partial M$. The last condition is equivalent to the complement of a small open regular neighborhood of $\mathcal{T}^0$ being homeomorphic to M. Henceforth, I will view M as embedded in $\mathcal{T}$ in this way, and as such M inherits a cell structure as a union of truncated tetrahedra.

Just as in the closed case, an acyclic edge orientation μ for $\mathcal{T}$ has an associated branched surface $B(\tau)$ defined by Figure 6, and I will always choose $B(\tau)$ so that it lies inside M. If $N(B(\tau))$ is the standard regular neighborhood of $B(\tau)$ as in [55, Sections 0–1], then $M \setminus \operatorname{int}\big(N(B(\tau))\big)$ is homeomorphic to $\partial M \times [0,1]$ and the vertical boundary $\partial_v N(B(\tau))$ forms a collection of annuli in $\partial M \times \{1\}$. The acyclic edge orientation μ is *persistently foliar* when all of these annuli are essential in ∂M and μ has no sink edges. When μ is persistently foliar, the annuli making up $\partial_v N(B(\tau))$ must all be parallel in $\partial M \times \{1\}$ and the common unoriented isotopy class of their core curves is called the *degeneracy slope* of μ, denoted by $\operatorname{degen}(\mu)$. The main result of this section is:

8.1 Theorem *Suppose M is a compact orientable 3–manifold with ∂M a torus with an ideal triangulation $\mathcal{T}$. If μ is a persistently foliar orientation for $\mathcal{T}$, then every Dehn filling $M(\alpha)$ of M with $\alpha \neq \operatorname{degen}(\mu)$ has a coorientable taut foliation.*

Proof of Theorem 8.1 The argument will closely parallel that given for Theorem 7.1. From now on, view $B = B(\mu)$ as a branched surface in $M(\alpha)$. I will first show that B is laminar. The guts $G = M(\alpha) \setminus \operatorname{int}(N(B))$ are a solid torus with both $\partial_h N(B)$ and $\partial_v N(B)$ being parallel annuli on ∂G which are essential because $\alpha \neq \operatorname{degen}(\mu)$. This immediately gives the first two criteria for B to be laminar, namely conditions (1) and (2) from Proposition 1.1 of [55]. The reason that B does not carry a surface that bounds a solid torus is essentially the same as in Theorem 7.1: every branch of B has nonzero algebraic intersection number with a closed loop in M, namely a loop

knot	description
$8n3$	torus knot $T(3,4)$
$10n21$	torus knot $T(3,5)$
$12n242$	$(-2,3,7)$ pretzel knot
$13n4587$	$(2,7)$ cable on $T(2,3)$
$13n4639$	$(2,5)$ cable on $T(2,3)$
$14n6022$	$(-2,3,9)$ pretzel knot
$14n21881$	torus knot $T(3,7)$
$15n40211$	$(2,9)$ cable on $T(2,3)$
$15n41185$	torus knot $T(4,5)$
$15n124802$	$(2,3)$ cable on $T(2,3)$
$16n184868$	$(-2,3,11)$ pretzel knot
$16n783154$	torus knot $T(3,8)$

Table 2: All 12 nonalternating L–space knots with at most 16 crossings. Nomenclature follows [50]. The above cables on the trefoil $T(2,3)$ are L–space knots by Theorem 1.10 of [44]. The pretzel knots are L–space knots by Theorem 1 of [3].

made by closing off a component of $\mathcal{T}^1 \cap M$ by an arc in ∂M. Finally, just as before the branched surface B has no sink discs since μ has no sink edges. So B is laminar.

As B is laminar, it carries an essential lamination by [55]. We can extend this lamination to a coorientable foliation $\mathcal{F}$ of all of $M(\alpha)$ by using the usual "stack of monkey saddles" or "stack of chairs" construction; see eg Example 4.22 of [15], and note we can extend the monkey saddles into $N(B)$ to fill up the remaining space since B has no discs of contact by Corollary 2.3 of [55]. It remains to check that $\mathcal{F}$ is taut. It is not hard to extend each arc in $\mathcal{T}^1 \cap M$ through the stack of monkey saddles to form a closed transverse loop, and together with the core curve of G we now have a collection of closed transverse loops meeting every leaf. Thus $M(\alpha)$ admits the taut foliation claimed. □

8.2 Exteriors of knots in the 3–sphere

The idea of constructing an object in a knot exterior M in S^3 that induces foliations in all but the trivial Dehn filling goes back at least to [30] and was used in [21; 60; 10; 45]

among others. In these references, the focus was on an essential lamination in M, called a *persistent lamination*, that remains essential in all nontrivial Dehn fillings. However, as in the proof of Theorem 8.1, in each Dehn filling one can fill up the complement of the lamination with monkey saddles to get a foliation. In the context of Theorem 8.1, the persistent lamination is carried by the branched surface $B(\tau)$. More generally, one can consider a certain class of *persistently foliar branched surfaces*, of which these $B(\tau)$ are examples, that give taut foliations on all nontrivial Dehn fillings of M.

A knot K in S^3 has a nontrivial Dehn surgery that is an L–space if and only if its exterior is Floer simple; knots with such surgeries are called L–space knots. Recently, Delman and Roberts have announced that such persistently foliar branched surfaces exist for all alternating knots and all Montesinos knots that have no L–space surgeries [22]. Motivated by this work, I tried to apply Theorem 8.1 to some nonalternating knots and found:

8.3 Theorem *Among the* 1 210 608 *nonalternating prime knots with at most* 16 *crossings, there are exactly* 12 *that are L–space knots. All the others have ideal triangulations of their exteriors with persistently foliar orientations; in particular, any nontrivial Dehn surgery on one of these knots admits a coorientable taut foliation.*

The 12 exceptions are listed in Table 2. This may seem like very few, but only 492 of these knots have Alexander polynomials with the form required by [63, Corollary 1.3] for being an L–space knot. The ideal triangulations used in Theorem 8.3 had between 5 and 39 tetrahedra, with a mean of 25.6; you can get all 1 210 596 ideal triangulations with persistent foliar orientations at [24] together with the relevant source code.

Combined with the work of Delman and Roberts [22], Theorem 8.3 makes it safe to posit:

8.4 Conjecture *The exterior of a non-L–space knot in S^3 has a persistently foliar branched surface.*

8.5 Examples

As with the closed case, persistently foliar orientations are quite common:

8.6 Theorem *At least* 8115 *of the manifolds in $\mathcal{C}$ have ideal triangulations that admit persistently foliar orientations.*

To put this in context, when M has a persistently foliar orientation, by Theorem 8.1 at most one Dehn filling of M can be an L–space and hence M is not Floer simple; by Remark 4.9, there are between 8352 and 8470 manifolds in $\mathcal{C}$ that are not Floer simple, so Theorem 8.6 covers at least 95.8% of them. Collectively, the foliar orientations in Theorem 8.6 give taut foliations on some 99 339 manifolds in $\mathcal{Y}$.

It is intriguing that every non-Floer simple knot exterior examined in Theorem 8.3 has a persistently foliar orientation, and yet there are non-Floer simple manifolds in $\mathcal{C}$ where I am unable to find such an orientation. This is particularly striking in light of the fact that the manifolds in Theorem 8.3 typically require many more tetrahedra to triangulate than those in $\mathcal{C}$. This suggests the answer to the following question might be yes:

8.7 Question Are there non-Floer simple manifolds that do not contain a persistently foliar branched surface?

The first few candidates in $\mathcal{C}$ for such a manifold are $v2347$, $v2626$, $v3452$, $t03447$, $t04027$, $t06287$, $t06400$, and $t06953$.

8.8 The manifold $m137$

Gao showed in [31] that the manifold $m137$ in $\mathcal{C}$ has infinitely many $\mathbb{Z}$–homology sphere fillings Y where $\pi_1(Y)$ has no nontrivial homomorphisms to $\mathrm{PSL}_2\mathbb{R}$. Thus, one cannot order $\pi_1(Y)$ using the technique of $\widetilde{\mathrm{PSL}_2\mathbb{R}}$–representations. However, the standard 4–tetrahedra triangulation of $m137$ has a persistently foliar orientation that shows that every Dehn filling except the homological longitude has a taut foliation. (The longitudinal filling is $S^2 \times S^1$.) In particular, each $\mathbb{Z}$–homology sphere filling Y has a taut foliation, and as $H^2(Y;\mathbb{Z}) = 0$, Theorem 9.1 from the next section applies to show that Y is orderable. So Gao's examples do fully satisfy Conjecture 1.2.

8.9 Collecting foliations

I now turn to:

Proof of Theorem 1.6(2) By Theorems 7.4 and 7.7, there are at least 160 177 manifolds in $\mathcal{Y}$ with taut foliations whose existence can be certified using a foliar orientation of the individual manifold. In addition, as per the discussion immediately after Theorem 8.6, some 99 339 manifolds in $\mathcal{Y}$ have taut foliations coming from persistently foliar orientations of manifolds in $\mathcal{C}$. Combined, these two methods cover 162 341 manifolds in $\mathcal{Y}$, completing the proof; see [24] for details. □

8.10 Remark Here is a sample of non-L–spaces where I was unable to find a taut foliation:

$$s137(5,4),\quad s460(6,1),\quad s593(6,1),\quad s614(5,1),\quad s753(-6,1),\quad s956(4,1),$$
$$v1333(-5,1),\quad v3045(-4,1),\quad t06114(5,1),\quad t08155(-5,1),$$
$$o9_{12518}(-6,1),\quad o9_{12544}(-4,3),\quad o9_{13679}(-6,1),\quad o9_{14675}(-1,5),$$
$$o9_{15066}(-5,1),\quad o9_{22743}(7,1),\quad o9_{30634}(6,1),\quad o9_{36699}(7,1).$$

I also do not know whether or not any of these manifolds are orderable.

9 Foliar orientations and the Euler class

The following is a consequence of Thurston's universal circle construction:

9.1 Theorem [8, Theorem 8.1] *A $\mathbb{Q}$–homology 3–sphere Y with a taut foliation $\mathcal{F}$ whose Euler class $e(\mathcal{F}) \in H^2(Y;\mathbb{Z})$ is zero is orderable.*

Roughly, Thurston associates to the taut foliation $\mathcal{F}$ an action of $\pi_1(Y)$ on a certain circle built from the circles at infinity of the induced foliation of the universal cover of Y; the Euler class of this action, which is the obstruction to lifting the action to $\mathbb{R}$, turns out to be $e(\mathcal{F})$. See Sections 6–8 of [8] for more.

Theorem 9.1 gives a very useful tool for showing a 3–manifold is orderable, and I now explain how to compute the Euler class for the foliation $\mathcal{F}$ associated to a foliar

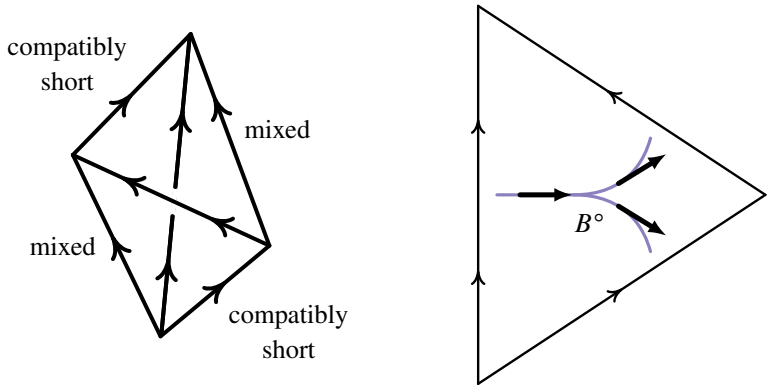

Figure 7: The mixed edges of an acyclically oriented tetrahedron (left) and the section η of UTB° in each face of $\mathcal{T}$ (right).

orientation μ. In any acyclically oriented tetrahedron, there are two edges that are short on one face but long on another; I will call these the *mixed* edges and they are shown in Figure 7, left. An edge $\tau \in \mathcal{T}^1$ appears as an edge in various of the tetrahedra in $\mathcal{T}^3$, and let $\operatorname{mixed}_\mu \tau$ be the number of times it appears as a mixed edge with respect to μ. (As $\mathcal{T}$ is not simplicial, the edge τ can appear several times in the same tetrahedron, and so a single tetrahedron could contribute as much as 2 to $\operatorname{mixed}_\mu \tau$.)

Consider the dual cell complex $\mathcal{D}$ to the triangulation $\mathcal{T}$ and orient the 2–cells of $\mathcal{D}$ by the orientation μ gives to the corresponding edge of $\mathcal{T}$. Define a cochain $\phi_\mu \in C^2(\mathcal{D}; \mathbb{Q})$ by

$$\phi_\mu(D) = 1 - \tfrac{1}{2} \operatorname{mixed}_\mu \tau \quad \text{where } \tau \in \mathcal{T}^1 \text{ is the edge dual to } D \in \mathcal{D}^2.$$

I will show:

9.2 Theorem *Suppose $\mathcal{F}$ is the foliation of Y associated to a foliar orientation μ of a 1–vertex triangulation $\mathcal{T}$. Then the cochain ϕ_μ is a cocycle lying in $C^2(\mathcal{D}; \mathbb{Z})$ and $[\phi_\mu] = e(\mathcal{F})$ in $H^2(\mathcal{D}; \mathbb{Z}) = H^2(Y; \mathbb{Z})$.*

Proof First, I will show that $e(\mathcal{F})$ is essentially just the Euler class of the tangent bundle to the branched surface $B = B(\mu)$. If we relax the condition that B has a well-defined tangent plane along its singular locus, then as a 2–complex B is isotopic to $\mathcal{D}^2$. As $\mathcal{T}$ has one vertex, the coboundary map $C^2(\mathcal{D}; \mathbb{Z}) \to C^3(\mathcal{D}; \mathbb{Z})$ is 0, and hence $B \hookrightarrow Y$ induces an isomorphism on H^i for $i \leq 2$. Thus $e(\mathcal{F}) \in H^2(Y; \mathbb{Z})$ is determined by the restriction of $T\mathcal{F}$ to B, which is bundle isomorphic to the tangent bundle TB. To prove the theorem, I will compute $e(TB)$ as the obstruction to the unit circle bundle $UTB \subset TB$ having a section; see eg [17, Chapter 4] for a detailed discussion of the Euler class along these lines.

Let B° be B with an open regular neighborhood of $\mathcal{T}^1$ removed. As B° deformation retracts to a graph, specifically one isotopic to $\mathcal{D}^1$, the restricted bundle UTB° necessarily has a section, and here is a concrete one. First, on $B^\circ \cap \mathcal{T}^2$ we take the section η that is tangent to the faces of $\mathcal{T}^2$ and within each face points away from the long edge as shown in Figure 7, right. Now extend η over all of B° using the template shown in Figure 8, where this includes using the mirrored picture when needed; the section η is roughly summarized by the rule that it points away from the very long edge.

Each component of $B \setminus B^\circ$ is a disc that is a shrunken copy of a face of $\mathcal{D}^2$. For each such disc D, fix a section δ of UTB over D. Thus we have two different

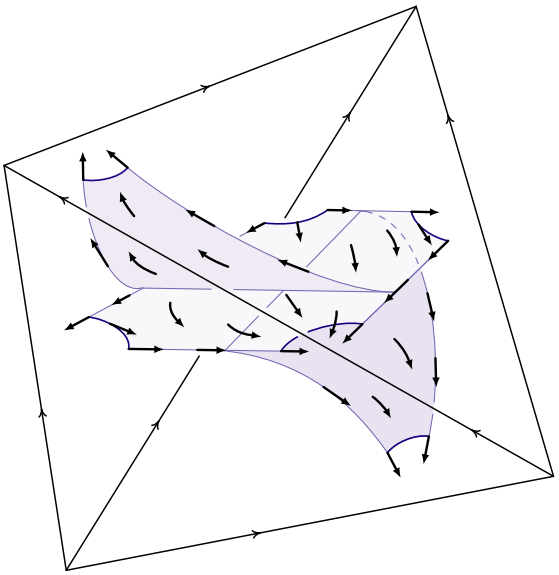

Figure 8: The section η of UTB° in each tetrahedron of $\mathcal{T}$.

sections of UTB over ∂D, namely the restrictions of δ and η. The usual cocycle for $e(TB)$ assigns to the face containing D the integer that expresses the difference between δ and η on ∂D. To compare these sections, consider a third section ν on ∂D that is normal to ∂D and points directly out of D and hence into B°. To understand how η compares to ν look at Figure 8 which contains six segments of ∂B°. On the segment near the very long edge, the section η is equal to ν, and there are three other segments where $\eta = -\nu$. The remaining two segments correspond to the mixed edges of the tetrahedron, and there η twists through half a turn with respect to ν. Now D gets an orientation from the face of $\mathcal{D}^2$ that contains it, which we use to orient ∂D as usual. Zooming in on the leftmost mixed edge of Figure 8, we get Figure 9, which shows that η does a *clockwise* twist on that segment with respect to ν. The same is true for the other mixed edge in Figure 8, as well the two mixed edges in the mirror image of Figure 8. Thus if D is dual to an edge $\tau \in \mathcal{T}^1$, we see that η twists through $\frac{1}{2}\operatorname{mixed}_\mu \tau$ clockwise full turns with respect to ν as you go around $\mathcal{D}$; in particular, the number $\frac{1}{2}\operatorname{mixed}_\mu \tau$ is in $\mathbb{Z}$. In contrast, the section δ that extends over D does one clockwise twist compared to ν. Thus the difference between η and δ on ∂D, expressed in terms of *anticlockwise* twists, is

$$\phi_\mu(D) = -\tfrac{1}{2}\operatorname{mixed}_\mu \tau + 1.$$

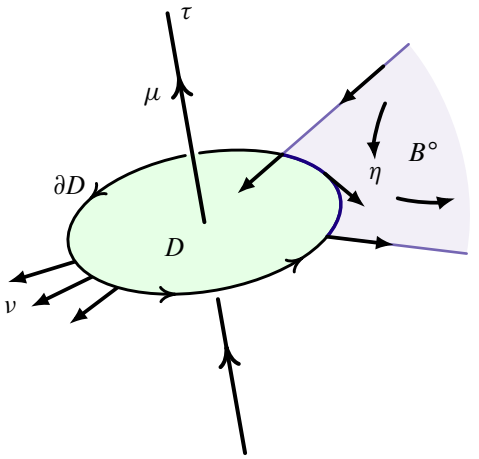

Figure 9: How η twists with respect to ν near a mixed edge τ.

To confirm that $\phi_\mu(D)$ is the obstruction to UTB having a section, simply note that if $\phi_\mu(D)$ is the coboundary of some one-chain $\alpha \in C^1(\mathcal{D};\mathbb{Z})$, then α gives instructions on how to twist η along the "arms" of B° (which correspond to the edges of $\mathcal{D}^1$) to get a new section that agrees with our section of UTB over $B \setminus B^\circ$ and hence gives a global section for UTB. Finally, to see that my conventions mean that $[\phi_\mu]$ represents $e(TB)$ rather than $-e(TB)$, simply carry out the corresponding calculation for eg TS^2. □

Applying this method to the sample at hand yields:

9.3 Theorem *At least 32 347 of the manifolds in $\mathcal{Y}$ have taut foliations whose Euler class vanishes and hence are orderable.*

Proof For Theorem 7.4, some 160 003 1–vertex triangulations were found for manifolds in $\mathcal{Y}$ that each had at least one foliar orientation. For each of these 3.5 million foliar orientations, I used Theorem 9.2 to determine whether the associated foliation had $e(\mathcal{F}) = 0$. There were 610 326 foliar orientations where $e(\mathcal{F}) = 0$, showing that some 32 347 manifolds in $\mathcal{Y}$ are orderable. The triangulations and the complete list of these foliar orientations are available at [24], as well as the code for computing the Euler class. □

9.4 Remark It is natural to ask to what extent $e(\mathcal{F})$ behaves like a random element of $H^2(Y;\mathbb{Z})$. Suppose that for each foliar orientation one has $e(\mathcal{F}) = 0$ with probability $1/|H^2(Y;\mathbb{Z})|$, and that the events $e(\mathcal{F}) = 0$ are independent for each foliar orientation.

Then for the 3.5 million foliar orientations in Theorem 7.4, the expected number with $e(\mathcal{F})=0$ is 276 602.7 and the expected number of Y with at least one foliar orientation with $e(\mathcal{F})=0$ is 67 595.3. (In both cases, the standard deviation is tiny by comparison: 416.4 and 149.6, respectively.) These predictions are off by about a factor of 2 in *opposite* directions from what was actually observed: 610 326 and 32 347. I have no explanation for this odd phenomenon.

9.5 Remark It would be very interesting to gauge the extent Theorem 9.3 finds all manifolds in $\mathcal{Y}$ with taut foliations whose Euler class vanishes. One approach here would be to refine the method of Section 4 so that it computes $\widehat{\mathrm{HF}}(Y)$ itself together with its Spin^c–grading as that provides obstructions to having taut foliations with particular Euler classes. For those Y that are Dehn fillings on Floer simple manifolds in $\mathcal{C}$, the methods of [64] should make this feasible using the Turaev torsion computations included in [24].

10 Representations to $\widetilde{\mathrm{PSL}_2\mathbb{R}}$

A very useful technique for showing a 3–manifold Y is orderable is to find a representation from $\pi_1(Y)$ to $\widetilde{\mathrm{PSL}_2\mathbb{R}}$, which is the universal covering Lie group of $\mathrm{PSL}_2\mathbb{R}$, and also its universal central extension (see eg [36, Section 5] or [11, Chapter 2]):

$$0\to\mathbb{Z}\to\widetilde{\mathrm{PSL}_2\mathbb{R}}\to\mathrm{PSL}_2\mathbb{R}\to 1.$$

The action of $\mathrm{PSL}_2\mathbb{R}$ on the circle $P^1(\mathbb{R})$ lifts to an action of $\widetilde{\mathrm{PSL}_2\mathbb{R}}$ on $\mathbb{R}$. If Y is an irreducible compact 3–manifold, then by Theorem 1.1 of [9] having a *nontrivial* representation $\rho\colon \pi_1(Y)\to\widetilde{\mathrm{PSL}_2\mathbb{R}}$ implies that Y is orderable. The last piece of Theorem 1.6 is:

10.1 Theorem *There are at least* 64 180 *manifolds $Y\in\mathcal{Y}$ where $\pi_1 Y$ has a nontrivial homomorphism to $\widetilde{\mathrm{PSL}_2\mathbb{R}}$; all these Y are therefore orderable.*

The manifolds in this theorem are all non-L–spaces, consistent with Conjecture 1.2.

10.2 Finding representations numerically

My starting point for Theorem 10.1 was numerical evidence of representations to $\widetilde{\mathrm{PSL}_2\mathbb{R}}$ coming from points on the extended Ptolemy variety that were computed

using numerical algebraic geometry. I now describe this method in detail. Throughout, let Y be a closed 3–manifold given as a Dehn filling on a manifold M with ∂M a torus, and suppose $\mathcal{T}$ is a fixed ideal triangulation of M. The first step is to find many (preferably all) representations $\pi_1(Y) \to \mathrm{PSL}_2\mathbb{C}$; later, these will be filtered to identify those that are conjugate into $\mathrm{PSL}_2\mathbb{R}$ and lift to $\widetilde{\mathrm{PSL}_2\mathbb{R}}$. Put another way, we need to compute the $\mathrm{PSL}_2\mathbb{C}$–character variety $X(Y)$, which is essentially representations $\pi_1(Y) \to \mathrm{PSL}_2\mathbb{C}$ modulo conjugacy and is an affine complex algebraic variety. For a relatively simple $\mathbb{Q}$–homology sphere like those in $\mathcal{Y}$, one expects that $\dim_{\mathbb{C}} X(Y) = 0$ and so there are only finitely many representations up to conjugacy.

Since $\pi_1(Y)$ is a quotient of $\pi_1(M)$, a representation of $\pi_1(Y)$ gives one of $\pi_1(M)$. A $\mathrm{PSL}_2\mathbb{C}$–representation of $\pi_1(M)$ can frequently be described in terms of the ideal triangulation $\mathcal{T}$. Specifically, if $\widetilde{\mathcal{T}}$ is the induced ideal triangulation of the universal cover of M, one tries to encode $\rho\colon \pi_1(M) \to \mathrm{PSL}_2\mathbb{C}$ by an equivariant developing map $\widetilde{\mathcal{T}} \to \mathbb{H}^3$ that takes each topological ideal tetrahedron of $\widetilde{\mathcal{T}}$ to a geodesic ideal tetrahedron in $\mathbb{H}^3$. (Technical aside: For some pairs $(\rho, \mathcal{T})$ no such developing map exists, and in practice one does lose some representations by taking this perspective; for ways around this limitation, which I did not use here, see [69; 38].) There are two ways of encoding such developing maps, both of which form algebraic varieties closely related to the character variety of M.

First, Thurston used one complex parameter for each tetrahedron in $\mathcal{T}$ to describe its geometric shape in $\mathbb{H}^3$, giving his *gluing equation variety* $D(\mathcal{T})$ which is cut out by one equation for each edge of $\mathcal{T}$; see eg [25, Section 3] for an overview and more on the map $D(\mathcal{T}) \to X(M)$. If α is the slope where $Y = M(\alpha)$, then by adding the cusp equation corresponding to α one obtains a subvariety $D(\mathcal{T}, \alpha)$ of $D(\mathcal{T})$. The subvariety $D(\mathcal{T}, \alpha)$ consists of all points mapping to $X(Y)$ together with those corresponding to representations of $\pi_1(M)$ where α acts by a nontrivial parabolic. More formally, if $X(M, \alpha)$ is the subset of $X(M)$ consisting of characters $[\rho]$ with $\mathrm{tr}^2(\rho(\alpha)) = 4$, then $D(\mathcal{T}, \alpha)$ is the preimage of $X(M, \alpha)$.

Second, the *enhanced Ptolemy variety* $P(\mathcal{T})$ for $\mathrm{PSL}_2\mathbb{C}$ uses one complex parameter for each edge of $\mathcal{T}$ as well as two such parameters for recording the eigenvalues of a basis of $\pi_1(\partial M)$; there is then one polynomial equation for each tetrahedron of $\mathcal{T}$. The basic Ptolemy variety was introduced in [35] and extended to nonboundary parabolic representations in [80] in the enhanced version used here, but I recommend the reader start with [34] which focuses on the case of $\mathrm{PSL}_2\mathbb{C}$ rather than the more general $\mathrm{SL}_n\mathbb{C}$

of [35]. To study the points of $P(\mathcal{T})$ mapping to $X(M,\alpha)$, one imposes an additional equation involving the two cusp parameters.

10.3 The Ptolemy advantage

The gluing and Ptolemy coordinates are in a certain sense dual [33, Section 12]. In particular, as $\mathcal{T}$ has the same number of edges as tetrahedra, both $D(\mathcal{T})$ and $P(\mathcal{T})$ live in $\mathbb{C}^n$ for roughly the same n. However, from the perspective of computational algebraic geometry there is a key difference between them: the equations defining $P(\mathcal{T})$ are typically much simpler than those defining $D(\mathcal{T})$. Specifically, they have much lower degrees. Both symbolic (eg Göbner bases) and numerical algorithms in algebraic geometry tend to be highly sensitive to the degree of the equations defining the variety. With the numerical method I used here, working with $P(\mathcal{T})$ was typically 10 times faster than using $D(\mathcal{T})$ and sometimes more than 50 times faster. Moreover, this was using a description of $D(\mathcal{T})$ with two variables per tetrahedron (representing z_i and $1-z_i$ in the usual parlance) which was itself 10 to 100 times faster than the standard description of $D(\mathcal{T})$ with just one variable per tetrahedron.

10.4 Finding points on the Ptolemy variety

In its simplest form, the Ptolemy variety parametrizes representations to $\mathrm{SL}_2\mathbb{C}$ rather than $\mathrm{PSL}_2\mathbb{C}$, though the latter case can be handled as well [34, Section 3]. Since a representation to $\mathrm{PSL}_2\mathbb{R}$ that lifts to $\widetilde{\mathrm{PSL}_2\mathbb{R}}$ necessarily lifts to the intermediate group $\mathrm{SL}_2\mathbb{R}$, I worked exclusively with the $\mathrm{SL}_2\mathbb{C}$ Ptolemy varieties. I used the *enhanced Ptolemy variety* of [80] to study representations of $\pi_1(M)$ that are not boundary-parabolic, specifically a variant of that construction due to Goerner (personal communication) that is easier to implement. I will use $P(\mathcal{T},\alpha)$ to denote the subset of the extended Ptolemy variety $P(\mathcal{T})$ where α acts by a matrix with eigenvalue 1. Using the peripheral holonomy map of [80, Section 4.2.2], one sees this adds a single equation, which if we take α to be our preferred meridian for ∂M, is simply the equation $m_1 = 1$ in the notation of [80].

While Goerner has had tremendous success computing the trace field of cusped hyperbolic 3–manifolds by applying exact symbolic methods to the Ptolemy variety [37], the equations in the closed case have higher degrees and for the manifolds in $\mathcal{Y}$ this seems to put the problem beyond the range where one can use Gröbner bases to find the solutions. Instead, I found many points on $P(\mathcal{T},\alpha)$ via the path homotopy continuation method

from numerical algebraic geometry (see [70, Sections 8.0–8.3] for general background), specifically the software PHCPack [76; 77]. In the form used, this method provides compelling numerical evidence of points on $P(\mathcal{T},\alpha)$ though it does not prove that any of the apparent solutions are close to actual solutions, and it can definitely miss some points with the parameters that I used. As mentioned above, one expects $X(Y)$ to be 0–dimensional, and similarly for $X(M,\alpha)$ and hence $P(\mathcal{T},\alpha)$. Thus I used PHCPack's algorithm for finding the isolated points of the input variety since that should typically be all of them here. The theory behind this is discussed in [70, Section 8.1], and I should point out that it requires having the same number of polynomial equations defining $P(\mathcal{T},\alpha)$ as there are variables. As mentioned, for $P(\mathcal{T},\alpha)$ we have one variable for each edge and two for the cusp, as well as one equation for each tetrahedron and a final equation for the cusp. This is actually one more variable than equation, but in fact one really works with the reduced Ptolemy variety [34, Section 4.1], which is equivalent to setting one edge parameter to 1, giving us a system of the required type. All of the Ptolemy coordinates must be nonzero, which puts $P(\mathcal{T},\alpha)$ into the "sparse system" setting of Table 8.1 of [70], where the number of points in the random starting system is determined by a mixed volume computation via the Bernshteĭn theory.

10.5 Numerical results

For each approximate point of $P(\mathcal{T},\alpha)$, the next step was to identify whether it gives an irreducible representation of $\pi_1(Y)$ whose image is moreover conjugate into $\mathrm{SL}_2\mathbb{R} \leq \mathrm{SL}_2\mathbb{C}$. For this, I converted over to the tetrahedra shape coordinates of $D(\mathcal{T})$ via [34, Equation (4-6)] and built the corresponding holonomy representation $\rho\colon \pi_1(M) \to \mathrm{SL}_2\mathbb{C}$ as in [25, Lemma 3.5]. To see if ρ factors through to $\pi_1(Y)$, I checked whether $\rho(\alpha) \approx I$. For the manifolds in $\mathcal{Y}$, this procedure identified some 27.8 million irreducible representations of their fundamental groups to $\mathrm{SL}_2\mathbb{C}$, an average of 90.5 per manifold. For each representation, I checked whether it is conjugate into SU_2 or $\mathrm{SL}_2\mathbb{R}$; see Table 3 for the resulting data. The running time for each manifold was typically between 10 seconds and a minute.

10.6 The Euler class and representations to $\widetilde{\mathrm{PSL}_2\mathbb{R}}$

For each representation ρ from $\pi_1(Y)$ to $\mathrm{SL}_2\mathbb{R}$, I computed the Euler class $e(\rho) \in H^2(Y;\mathbb{Z})$ of the induced action on the circle, which is also the obstruction to lifting ρ to $\widetilde{\rho}\colon \pi_1(Y) \to \widetilde{\mathrm{PSL}_2\mathbb{R}}$. The Euler class vanished for 113 721 (4.7%) of the $\mathrm{SL}_2\mathbb{R}$–representations, providing compelling numerical evidence that some 68 054 manifolds

	$\mathrm{SL}_2\mathbb{C}$	SU_2	$\mathrm{SL}_2\mathbb{R}$	$\widetilde{\mathrm{PSL}_2\mathbb{R}}$
L–spaces	103.2	22.8	9.2	0.0
non-L–spaces	79.3	21.4	6.6	0.7

Table 3: This table shows the average number of irreducible representations of $\pi_1(Y)$ for $Y \in \mathcal{Y}$ found in Section 10.5 for various target groups, separated out by whether the manifold is an L–space or not. Representations to SU_2 and $\mathrm{SL}_2\mathbb{R}$ are also counted in the $\mathrm{SL}_2\mathbb{C}$ column, so eg the average number of Zariski dense representations to $\mathrm{SL}_2\mathbb{C}$ for an L–space was 71.2.

in $\mathcal{Y}$ are orderable. All of the apparently orderable manifolds are non-L–spaces, and I will prove they are indeed orderable in the vast majority (94.3%) of cases in Section 11.

10.7 Remark As with Remark 9.4, it is natural to ask to what extent $e(\rho)$ behaves like a random element of $H^2(Y;\mathbb{Z})$. If it were random, the expected number of ρ with $e(\rho)=0$ would be 64 530, whereas the observed number is 76.2% more than that. That is, the Euler class was more likely to vanish than the size of $H^2(Y;\mathbb{Z})$ would suggest. However, if we look at just the L–spaces, the opposite is very much the case: if $e(\rho)=0$ with probability $1/|H^2(Y;\mathbb{Z})|$, the expected number of ρ with $e(\rho)=0$ and where Y is an L–space is 6318, which is much larger than the zero such ρ observed. Indeed, the probability that a random $e(\rho)$ is nonzero whenever Y is an L–space in this sample is less than 10^{-2700}. This is quite good evidence for the conjecture that L–spaces are not orderable!

Given that more than half the manifolds in $\mathcal{Y}$ are L–spaces, you might wonder why one expects only 6318 cases where $e(\rho)=0$ for L–spaces and 58 212 such cases for non-L–spaces. While Table 3 shows that L–spaces average 39.4% more representations to $\mathrm{SL}_2\mathbb{R}$ than non-L–spaces, their homology was on average much larger, with a mean size of 257.5 versus 61.2.

11 Proving orderability

This section gives the proof of Theorem 10.1. As in Section 10, let Y be a closed 3–manifold given as the Dehn filling $M(\alpha)$ with $\mathcal{T}$ a fixed ideal triangulation of M. The first step will be to adapt the interval analysis methods of Section 6.1 to certify a solution to the gluing equations of $\mathcal{T}$ where the associated holonomy representation has image in $\mathrm{PSL}_2\mathbb{R}$.

11.1 Shapes giving $\mathrm{PSL}_2\mathbb{R}$–representations

Consider a solution to Thurston's gluing equations, that is, a point $z \in D(\mathcal{T}, \alpha) \subset \mathbb{C}^n$, with associated representation $\rho\colon \pi_1(M) \to \mathrm{PSL}_2\mathbb{C}$. When can we conjugate ρ so that the image is in $\mathrm{PSL}_2\mathbb{R}$? If all the shapes are real and so $z \in \mathbb{R}^n$, we can choose the associated developing map $\widetilde{\mathcal{T}} \to \mathbb{H}^3$ to have image in our preferred copy of $\mathbb{H}^2 \subset \mathbb{H}^3$ and hence ρ will preserve $\mathbb{H}^2$ as well. In this case, the image of ρ is contained in the stabilizer of $\mathbb{H}^2$ in $\mathrm{PSL}_2\mathbb{C}$, which is the full isometry group of $\mathbb{H}^2$ and contains $\mathrm{PSL}_2\mathbb{R}$ as its identity component. For any generating set $\{\gamma_i\}$ of $\pi_1(M)$, when all $\mathrm{tr}(\rho(\gamma_i))$ are real (as opposed to some being purely imaginary), it means ρ has image in $\mathrm{PSL}_2\mathbb{R}$. However, it is possible to have some nonreal shapes and yet ρ is still conjugate into $\mathrm{PSL}_2\mathbb{R}$. Indeed, for a $\mathrm{PSL}_2\mathbb{R}$–representation where some element of $\pi_1(\partial M)$ acts by an elliptic element, it is impossible for all the shapes to be real, and this was the case for 69.0% of the $\mathrm{SL}_2\mathbb{R}$–representations in Table 3 that lifted to $\widetilde{\mathrm{PSL}_2\mathbb{R}}$–representations. That said, if $\rho(\pi_1(\partial M))$ contains a hyperbolic or parabolic element then ρ is conjugate into the stabilizer of $\mathbb{H}^2$ if and only if $z \in \mathbb{R}^n$.

11.2 Certifying real representations

To use the approach of [47] to certify $\mathrm{PSL}_2\mathbb{R}$–representations, it is easiest to work only with real shapes. As only 31% of the candidate $\widetilde{\mathrm{PSL}_2\mathbb{R}}$–representations identified in Section 10.6 had this property, I looked at other Dehn filling descriptions of each Y found by drilling out various short curves. Any irreducible $\rho\colon \pi_1(Y) \to \mathrm{PSL}_2\mathbb{R}$ always sends some element to a hyperbolic one, so drilling out such a loop is likely to yield a triangulation where ρ will be exhibited by real shapes. I succeeded in finding an alternate description of Y with a representation to $\widetilde{\mathrm{PSL}_2\mathbb{R}}$ coming from real shapes in 94.3% of cases, though this required working with triangulations with as many as 13 tetrahedra.

Let $\mathrm{I}\mathbb{R}$ denote the set of real intervals with rational endpoints. For a point in $\mathbb{R}^n$ that appears to approximate a point in $D(\mathcal{T}, \alpha)$, the first step is to modify Section 6.1 to give a criterion for showing a nearby $\boldsymbol{z} \in \mathrm{I}\mathbb{R}^n$ is guaranteed to contain a point of $z \in D(\mathcal{T}, \alpha)$. To do this, we simply replace $\mathrm{I}\mathbb{C}$ with $\mathrm{I}\mathbb{R}$ and use the rectangular form of the gluing equations rather than the logarithmic one. The subtle point is that we need to check that the associated ρ has $\rho(\alpha) = I$ as opposed to $\rho(\alpha)$ being parabolic. In Section 6.1, this follows geometrically because the shapes have positive imaginary component and the log-holonomy of α is $2\pi i$. In the current case, I instead computed the approximate

$\mathrm{PSL}_2\mathbb{R}$–representation $\boldsymbol{\rho}\colon \pi_1(M)\to \mathrm{PGL}_2\mathrm{I}\mathbb{R}$ analogous to what is built in Section 6.2 and checked that $\mathrm{tr}^2\,\boldsymbol{\rho}(\beta)>4$ for some slope $\beta\neq\alpha$. This last condition forces the underlying $\rho(\beta)$ to be hyperbolic, and so $\rho(\alpha)$ must be I because $\rho(\alpha)$ and $\rho(\beta)$ commute. (Aside: If $\rho(\alpha)$ is instead parabolic, we can usually confirm this by showing $\boldsymbol{\rho}(\alpha)$ does not contain I. The remaining ambiguous cases, eg when $\rho(\alpha)$ is trivial and $\rho(\beta)$ is parabolic, are probably best handled by changing the Dehn filling description.) Thus, at the end one has a $\boldsymbol{\rho}\colon \pi_1(Y)\to \mathrm{PSL}_2\mathrm{I}\mathbb{R}$ that is certified to contain some actual representation $\rho\colon \pi_1(Y)\to \mathrm{PSL}_2\mathbb{R}$, which must be nontrivial since at least one $\rho(\beta)$ is hyperbolic. Moreover, we can lift ρ to $\widetilde{\rho}\colon \pi_1(Y)\to \mathrm{SL}_2\mathbb{R}$ when $\pi_1(Y)=\langle S \mid R_1,\dots,R_n\rangle$ if we can chose a lift $\widetilde{\boldsymbol{\rho}}\colon S\to \mathrm{SL}_2\mathrm{I}\mathbb{R}$ such that $-2\notin \mathrm{tr}(\widetilde{\boldsymbol{\rho}}(R_i))$ for all i. Here, since I started with shapes coming from an approximate point in the $\mathrm{SL}_2\mathbb{C}$ Ptolemy variety, I unsurprisingly always succeeded in finding such a lift.

11.3 Lifting representations

For ease of notation, let $G=\mathrm{SL}_2\mathbb{R}$, $\mathrm{I}G=\mathrm{SL}_2\mathrm{I}\mathbb{R}$, and $\widetilde{G}=\widetilde{\mathrm{PSL}_2\mathbb{R}}$. Also set $\Gamma=\pi_1(Y)$ with $\langle S \mid R_1,\dots,R_n\rangle$ a finite presentation for Γ. Given $\boldsymbol{\rho}\colon S\to \mathrm{I}G$, which is guaranteed to contain a representation $\rho\colon \Gamma\to G$, we need a way to show that ρ lifts to $\widetilde{G}$ under

$$0\to\mathbb{Z}\to\widetilde{G}\to G\to 1$$

by a computation using only $\boldsymbol{\rho}$. A 2–cocycle c representing the obstruction $e(\rho)\in H^2(\Gamma;\mathbb{Z})$ to ρ lifting can be defined by choosing any lift $\widetilde{\rho}\colon \mathrm{FreeGroup}(S)\to\widetilde{G}$ of $\rho|_S$ and setting $c(R_i)=\widetilde{\rho}(R_i)$, which is in the center $\mathbb{Z}$ of $\widetilde{G}$. Thus, the key issue is how to work in $\widetilde{G}$ starting from our approximate representation $\boldsymbol{\rho}$.

11.4 Working with $\widetilde{G}$

As $\widetilde{G}$ is nonlinear, ie cannot be embedded in any $\mathrm{GL}_n\mathbb{R}$, it is not easy to work with computationally, especially as we need to do so rigorously in the context of interval arithmetic. I used the following approach, motivated by [11, Chapter 2], which you can consult for additional details. In this section, we identify the hyperbolic plane $\mathbb{H}^2$ with $\{z\in\mathbb{C}\mid \mathrm{Im}(z)>0\}$ and focus on the Möbius action of G on $\mathbb{H}^2$. The stabilizer of $i\in\mathbb{H}^2$ is

$$K=\left\{\hat{k}(t)=\begin{pmatrix}\cos t & \sin t\\ -\sin t & \cos t\end{pmatrix}\;\middle|\; t\in\mathbb{R}/2\pi\mathbb{Z}\right\},$$

where $\widehat{k}(t)$ rotates anticlockwise around the point i through angle $2t$. The stabilizer of $\infty \in \partial\mathbb{H}^2$ is

$$P = \left\{ \widehat{p}(z) = \begin{pmatrix} \sqrt{y} & \frac{x}{\sqrt{y}} \\ 0 & \frac{1}{\sqrt{y}} \end{pmatrix} \,\middle|\, z = x + iy \in \mathbb{H}^2 \right\},$$

where $\widehat{p}(z)$ takes i to z. Any element $g = \left(\begin{smallmatrix} a & b \\ c & d \end{smallmatrix}\right)$ in G can be uniquely written as $\widehat{p}(z)\widehat{k}(t)$ where $z = g \cdot i$ and $\widehat{k}(t) = \widehat{p}(z)^{-1} g$ or alternatively $t = \arg(d - ic)$. The map $P \times K \to G$ taking (p, k) to $p \cdot k$ is a diffeomorphism, showing $G \cong \mathbb{H}^2 \times S^1$ as analytic manifolds. The universal covering group $\widetilde{G}$ is thus topologically $\mathbb{H}^2 \times \mathbb{R}$. Taking $\widetilde{P} \subset \widetilde{G}$ to be the preimage of P, the map $\widetilde{P} \to P$ is a group isomorphism, and we define $p(z) \in \widetilde{P}$ to be the element mapping to $\widehat{p}(z)$. The preimage $\widetilde{K}$ of K is isomorphic to $(\mathbb{R}, +)$ with $\widetilde{K} \to K$ having kernel $2\pi\mathbb{Z}$; we denote the elements of $\widetilde{K}$ by $p(t)$ for $t \in \mathbb{R}$ where $p(t) \cdot p(t') = p(t + t')$ and $p(t) \mapsto \widehat{p}(t)$. Thus each element of $\widetilde{G}$ can be uniquely expressed in the form $p(z)k(t)$ for some $z \in \mathbb{H}^2$ and $t \in \mathbb{R}$. I will record a $\widetilde{g} \in \widetilde{G}$ by the pair $(g, t) \in G \times \mathbb{R}$ where $\widetilde{g} \mapsto g$ and t is the $\widetilde{K}$–coordinate of $\widetilde{g}$; concretely, this identifies $\widetilde{G}$ with

$$\left\{ \left(\begin{pmatrix} a & b \\ c & d \end{pmatrix}, t \right) \in G \times \mathbb{R} \,\middle|\, \frac{d - ic}{\sqrt{c^2 + d^2}} = e^{it} \right\}. \tag{11.5}$$

If g and g' are in G, then setting $z' = g \cdot i$ it follows from [11, page 28] that the group law on $\widetilde{G}$ can be written

$$(g, t) \cdot (g', t') = \big(g \cdot g',\ t + t' - \arg(e^{it}(-z' \sin t + \cos t))\big), \tag{11.6}$$

where here arg takes values in $(-\pi, \pi]$; one can show the input to arg is never in $(-\infty, 0] \subset \mathbb{C}$, so this term is in fact continuous (indeed analytic) in z' and t. (In contrast, the book [11] uses (z, t) as coordinates on $\widetilde{G}$, which is more concise but the formula for the z part of the group law is then more complicated than just multiplying matrices.)

11.7 An interval version of $\widetilde{G}$

Motivated by the description (11.5) for $\widetilde{G}$, define $\mathrm{I}\widetilde{G}$ to be

$$\left\{ \left(\begin{pmatrix} \boldsymbol{a} & \boldsymbol{b} \\ \boldsymbol{c} & \boldsymbol{d} \end{pmatrix}, \boldsymbol{t} \right) \in (M_2\,\mathrm{I}\mathbb{R}) \times \mathrm{I}\mathbb{R} \,\middle|\, \begin{array}{l} \text{there exist interval reps } a, b, c, d, t \in \mathbb{R} \text{ such} \\ \text{that } ad - bc = 1 \text{ and } (d - ic)/\sqrt{c^2 + d^2} = e^{it} \end{array} \right\},$$

where here $a \in \boldsymbol{a}$, $b \in \boldsymbol{b}$, etc. We can view $\widetilde{G}$ as a subset of $\mathrm{I}\widetilde{G}$, and given an element $\boldsymbol{g} = \left(\begin{smallmatrix} \boldsymbol{a} & \boldsymbol{b} \\ \boldsymbol{c} & \boldsymbol{d} \end{smallmatrix}\right)$ in $\mathrm{SL}_2\mathrm{I}\mathbb{R}$ known to contain a $g \in \mathrm{SL}_2\mathbb{R}$, then $(\boldsymbol{g}, \boldsymbol{t})$ is in $\mathrm{I}\widetilde{G}$ if we take

$$\boldsymbol{t} = \arg((\boldsymbol{d} - i\,\boldsymbol{c})/\sqrt{\boldsymbol{c}^2 + \boldsymbol{d}^2}). \tag{11.8}$$

Using (11.6), we can multiply elements $(\boldsymbol{g}, \boldsymbol{t})$ and $(\boldsymbol{g}', \boldsymbol{t}')$ of $\mathrm{I}\widetilde{G}$ together provided the element of $\mathrm{I}\mathbb{C}$

$$\boldsymbol{r} = e^{i\boldsymbol{t}}(-\boldsymbol{z}' \sin \boldsymbol{t} + \cos \boldsymbol{t}) \quad \text{where } \boldsymbol{z}' = \boldsymbol{g}' \cdot i$$

is disjoint from $(-\infty, 0]$, which is something that can be easily checked from the four corners of the rectangle $\boldsymbol{r}$.

11.9 Proof of Theorem 10.1

For 64 180 manifolds Y in $\mathcal{Y}$, I found a Dehn surgery description $Y = M(\alpha)$ where M had an ideal triangulation $\mathcal{T}$ with n tetrahedra with a point $z_0 \in \mathbb{R}^n$ where the following held. First, the method of Section 11.2 showed there was a point in $D(\mathcal{T}, \alpha)$ near z_0 such that the associated $\rho\colon \pi_1(M) \to \mathrm{PSL}_2\mathbb{R}$ factored through to $\pi_1(Y)$, was nontrivial, and lifted to $G = \mathrm{SL}_2\mathbb{R}$. Second, starting from the approximate representation $\boldsymbol{\rho}\colon \pi_1(Y) \to \mathrm{I}G$ and a presentation $\pi_1(Y) = \langle S \mid R_1, \dots, R_n \rangle$, I constructed a lift $\widetilde{\boldsymbol{\rho}}\colon \mathrm{FreeGroup}(S) \to \mathrm{I}\widetilde{G}$ of $\boldsymbol{\rho}|_S$ by setting $\widetilde{\boldsymbol{\rho}}(\gamma) = (\boldsymbol{\rho}(\gamma), \boldsymbol{t})$, where $\boldsymbol{t}$ is defined by (11.8). For each relator R_i, one must have that $\widetilde{\boldsymbol{\rho}}(R_i) = (\boldsymbol{g}, \boldsymbol{t})$ contains an element of the center of $\widetilde{G}$, that is $I \in \boldsymbol{g}$ and $\boldsymbol{t} \cap 2\pi\mathbb{Z} \neq \varnothing$. Provided there is a unique $m \in \mathbb{Z}$ with $2\pi m \in \boldsymbol{t}$, it follows that the 2–cocycle for $e(\rho)$ described in Section 11.3 takes the value m on R_i. I then checked that this cocycle was a coboundary. This proved the existence of a nontrivial representation $\widetilde{\rho}\colon \pi_1(Y) \to \widetilde{G}$ and hence Y is orderable.

As in Section 6.6, the amount of precision needed varied, both to certify the initial solution and to avoid the branch cut of arg when computing in IG. In 95% of the cases, using 200 bits of precision sufficed, but the hardest 67 examples required 1000 bits. For each Y, the precise Dehn surgery description, triangulation, the approximate shapes, and level of precision are available at [24] along with the code used to check them all. This completes the proof of Theorem 10.1.

11.10 Proof of Theorem 1.6(3)

Theorems 9.3 and 10.1 respectively show that at least 32 347 and 64 180 manifolds in $\mathcal{Y}$ are orderable. From [24], we can determine the overlap between the two methods,

and find that at least one of these theorems applies to some 80 236 of them. Comparing with the data behind Theorem 1.6(1) confirms that these are all non-L–spaces, proving Theorem 1.6(3).

12 Code and data

The full data and code for all these proofs is permanently archived on the Harvard Dataverse [24]. One method I used to try to ensure the correctness of the code is worth mentioning. The results of Theorem 1.6 about the manifolds $Y \in \mathcal{Y}$ came from:

(1) Determining which Y are L–spaces using Section 4.

(2) Showing Y is not orderable using Section 5.

(3) Finding taut foliations from foliar orientations (Sections 7 and 8) and using these to show Y is orderable (Section 9).

(4) Showing Y is orderable using representations to $\widetilde{\mathrm{PSL}_2\mathbb{R}}$ (Section 11).

The only place where information from one part was used in another is that 4% of the foliations found in (3) were used in (1) to show the last stubborn 2.1% of manifolds in $\mathcal{Y}$ were not L–spaces. Putting aside this 2.1%, the above items represent four completely independent programs. The key safeguard is that all four programs were run on the *whole* of $\mathcal{Y}$, even though this meant huge amounts of time was spent searching for foliar orientations on manifolds already known to be L–spaces, searching for orders of manifolds already known not to have any, etc. Rather that being a waste of computational resources, this represents compelling evidence for the correctness of the code since no contradictory results were obtained! For example, suppose that the program in (1) had a bug causing it to randomly output the wrong answer for 1 in every 10 000 inputs. We would then expect about 16 manifolds in $\mathcal{Y}$ for which a taut foliation would have been found in (3) but that were reported in (1) as L–spaces, which is of course impossible [62]. Indeed, the probability that no such "L–space with a taut foliation" was found with these assumptions is less than 10^{-7}. Hence, one should expect that the probability that the program in (1) reports non-L–spaces as L–spaces is well less than 10^{-4}.

References

[1] **I Agol**, *Virtual properties of* 3*–manifolds*, from "Proceedings of the International Congress of Mathematicians, I" (S Y Jang, Y R Kim, D-W Lee, I Ye, editors), Kyung Moon Sa, Seoul (2014) 141–170 MR

[2] **I Agol**, **T Li**, *An algorithm to detect laminar 3–manifolds*, Geom. Topol. 7 (2003) 287–309

[3] **K L Baker**, **A H Moore**, *Montesinos knots, Hopf plumbings, and L–space surgeries*, J. Math. Soc. Japan 70 (2018) 95–110 MR

[4] **W Bosma**, **J Cannon**, **C Playoust**, *The Magma algebra system, I: The user language*, J. Symbolic Comput. 24 (1997) 235–265 MR

[5] **J Bowden**, *Approximating C^0–foliations by contact structures*, Geom. Funct. Anal. 26 (2016) 1255–1296 MR

[6] **S Boyer**, **A Clay**, *Foliations, orders, representations, L–spaces and graph manifolds*, Adv. Math. 310 (2017) 159–234 MR

[7] **S Boyer**, **C M Gordon**, **L Watson**, *On L–spaces and left-orderable fundamental groups*, Math. Ann. 356 (2013) 1213–1245 MR

[8] **S Boyer**, **Y Hu**, *Taut foliations in branched cyclic covers and left-orderable groups*, Trans. Amer. Math. Soc. 372 (2019) 7921–7957 MR

[9] **S Boyer**, **D Rolfsen**, **B Wiest**, *Orderable 3–manifold groups*, Ann. Inst. Fourier (Grenoble) 55 (2005) 243–288 MR

[10] **M Brittenham**, *Persistent laminations from Seifert surfaces*, J. Knot Theory Ramifications 10 (2001) 1155–1168 MR

[11] **R W Bruggeman**, *Families of automorphic forms*, Monogr. Math. 88, Birkhäuser, Boston (1994) MR

[12] **B A Burton**, *The cusped hyperbolic census is complete*, preprint (2014) arXiv

[13] **B A Burton**, **R Budney**, **W Pettersson**, et al., *Regina: software for low-dimensional topology* (1999) Available at `http://regina-normal.github.io`

[14] **D Calegari**, *Foliations transverse to triangulations of 3–manifolds*, Comm. Anal. Geom. 8 (2000) 133–158 MR

[15] **D Calegari**, *Foliations and the geometry of 3–manifolds*, Oxford Univ. Press (2007) MR

[16] **D Calegari**, **N M Dunfield**, *Laminations and groups of homeomorphisms of the circle*, Invent. Math. 152 (2003) 149–204 MR

[17] **A Candel**, **L Conlon**, *Foliations, II*, Grad. Stud. Math. 60, Amer. Math. Soc., Providence, RI (2003) MR

[18] **A Clay**, **D Rolfsen**, *Ordered groups and topology*, Grad. Stud. Math. 176, Amer. Math. Soc., Providence, RI (2016) MR

[19] **M Culler**, **N M Dunfield**, *Orderability and Dehn filling*, Geom. Topol. 22 (2018) 1405–1457 MR

[20] **M Culler**, **N M Dunfield**, **J R Weeks**, *SnapPy, a computer program for studying the topology of 3–manifolds* Available at `http://snappy.computop.org`

[21] **C Delman**, *Essential laminations and Dehn surgery on 2–bridge knots*, Topology Appl. 63 (1995) 201–221 MR

[22] **C Delman**, **R Roberts**, *Alternating knots and Montesinos knots satisfy the L–space knot conjecture*, video lecture presented by Delman, Univ. Illinois (2017) Available at `https://youtu.be/1M8NvoiDGzc`

[23] **N M Dunfield**, *A census of exceptional Dehn fillings* (2018) arXiv To appear in "Characters in low-dimensional topology" (O Collin, S Friedl, C Gordon, S Tillmann, L Watson, editors), Contemp. Math. 760, Amer. Math. Soc., Providence, RI

[24] **N Dunfield**, code and data to accompany this paper, Harvard Dataverse (2019) Available at `https://doi.org/10.7910/DVN/LCYXPO`

[25] **N M Dunfield**, **S Garoufalidis**, *Incompressibility criteria for spun-normal surfaces*, Trans. Amer. Math. Soc. 364 (2012) 6109–6137 MR

[26] **N M Dunfield**, **N R Hoffman**, **J E Licata**, *Asymmetric hyperbolic L–spaces, Heegaard genus, and Dehn filling*, Math. Res. Lett. 22 (2015) 1679–1698 MR

[27] **D B A Epstein**, **J W Cannon**, **D F Holt**, **S V F Levy**, **M S Paterson**, **W P Thurston**, *Word processing in groups*, Jones & Bartlett, Boston (1992) MR

[28] **W Floyd**, **B Weber**, **J Weeks**, *The Achilles' heel of* $\mathrm{O}(3,1)$*?*, Experiment. Math. 11 (2002) 91–97 MR

[29] **D Gabai**, *Combinatorial volume preserving flows and taut foliations*, Comment. Math. Helv. 75 (2000) 109–124 MR

[30] **D Gabai**, **W H Kazez**, *Pseudo-Anosov maps and surgery on fibred 2–bridge knots*, Topology Appl. 37 (1990) 93–100 MR

[31] **X Gao**, *Non-L–space integral homology 3–spheres with no nice orderings*, Algebr. Geom. Topol. 17 (2017) 2511–2522 MR

[32] **G Gardam**, *Profinite rigidity in the SnapPea census*, Experiment. Math. (online publication April 2019)

[33] **S Garoufalidis**, **M Goerner**, **C K Zickert**, *Gluing equations for* $\mathrm{PGL}(n,\mathbb{C})$*–representations of 3–manifolds*, Algebr. Geom. Topol. 15 (2015) 565–622 MR

[34] **S Garoufalidis**, **M Goerner**, **C K Zickert**, *The Ptolemy field of 3–manifold representations*, Algebr. Geom. Topol. 15 (2015) 371–397 MR

[35] **S Garoufalidis**, **D P Thurston**, **C K Zickert**, *The complex volume of* $\mathrm{SL}(n,\mathbb{C})$*–representations of 3–manifolds*, Duke Math. J. 164 (2015) 2099–2160 MR

[36] **É Ghys**, *Groups acting on the circle*, Enseign. Math. 47 (2001) 329–407 MR

[37] **M Goerner**, *Ptolemy data for SnapPy manifolds* Available at `http://tinyurl.com/goerner-ptolemy-data`

[38] **M Goerner**, **C K Zickert**, *Triangulation independent Ptolemy varieties*, Math. Z. 289 (2018) 663–693 MR

[39] **C Gordon**, **T Lidman**, *Taut foliations, left-orderability, and cyclic branched covers*, Acta Math. Vietnam. 39 (2014) 599–635 MR

[40] **J Hanselman**, *Bordered Heegaard Floer homology and graph manifolds*, Algebr. Geom. Topol. 16 (2016) 3103–3166 MR

[41] **J Hanselman**, *HFhat_graph_manifolds* (2016) Python package Available at `https://github.com/hanselman/HFhat_graph_manifolds`

[42] **J Hanselman**, **J Rasmussen**, **S D Rasmussen**, **L Watson**, *L–spaces, taut foliations, and graph manifolds*, Compos. Math. 156 (2020) 604–612 MR

[43] **A Hatcher**, *Algebraic topology*, Cambridge Univ. Press (2002) MR

[44] **M Hedden**, *On knot Floer homology and cabling, II*, Int. Math. Res. Not. 2009 (2009) 2248–2274 MR

[45] **M Hirasawa**, **T Kobayashi**, *Pre-taut sutured manifolds and essential laminations*, Osaka J. Math. 38 (2001) 905–922 MR

[46] **C D Hodgson**, **J R Weeks**, *Symmetries, isometries and length spectra of closed hyperbolic three-manifolds*, Experiment. Math. 3 (1994) 261–274 MR

[47] **N Hoffman**, **K Ichihara**, **M Kashiwagi**, **H Masai**, **S Oishi**, **A Takayasu**, *Verified computations for hyperbolic 3–manifolds*, Experiment. Math. 25 (2016) 66–78 MR

[48] **N R Hoffman**, **G S Walsh**, *The big Dehn surgery graph and the link of S^3*, Proc. Amer. Math. Soc. Ser. B 2 (2015) 17–34 MR

[49] **D F Holt**, **B Eick**, **E A O'Brien**, *Handbook of computational group theory*, Chapman & Hall, Boca Raton, FL (2005) MR

[50] **J Hoste**, **M Thistlethwaite**, **J Weeks**, *The first 1,701,936 knots*, Math. Intelligencer 20 (1998) 33–48 MR

[51] **F Johansson**, *Arb: efficient arbitrary-precision midpoint-radius interval arithmetic*, IEEE Trans. Comput. 66 (2017) 1281–1292 MR

[52] **A Juhász**, *A survey of Heegaard Floer homology*, from "New ideas in low dimensional topology" (L H Kauffman, V O Manturov, editors), Ser. Knots Everything 56, World Sci., Hackensack, NJ (2015) 237–296 MR

[53] **W H Kazez**, **R Roberts**, *C^0 approximations of foliations*, Geom. Topol. 21 (2017) 3601–3657 MR

[54] **P Kronheimer**, **T Mrowka**, **P Ozsváth**, **Z Szabó**, *Monopoles and lens space surgeries*, Ann. of Math. 165 (2007) 457–546 MR

[55] **T Li**, *Laminar branched surfaces in 3–manifolds*, Geom. Topol. 6 (2002) 153–194 MR

[56] **R Lipshitz**, **P S Ozsváth**, **D P Thurston**, *Bordered Heegaard Floer homology: invariance and pairing*, preprint (2008) arXiv

[57] **R Lipshitz**, **P S Ozsváth**, **D P Thurston**, *Tour of bordered Floer theory*, Proc. Natl. Acad. Sci. USA 108 (2011) 8085–8092 MR

[58] **K Matsuzaki**, **M Taniguchi**, *Hyperbolic manifolds and Kleinian groups*, Oxford Univ. Press (1998) MR

[59] **R E Moore**, **R B Kearfott**, **M J Cloud**, *Introduction to interval analysis*, SIAM, Philadelphia (2009) MR

[60] **R Naimi**, *Constructing essential laminations in 2–bridge knot surgered 3–manifolds*, Pacific J. Math. 180 (1997) 153–186 MR

[61] **W D Neumann**, *A calculus for plumbing applied to the topology of complex surface singularities and degenerating complex curves*, Trans. Amer. Math. Soc. 268 (1981) 299–344 MR

[62] **P Ozsváth**, **Z Szabó**, *Holomorphic disks and genus bounds*, Geom. Topol. 8 (2004) 311–334 MR

[63] **P Ozsváth**, **Z Szabó**, *On knot Floer homology and lens space surgeries*, Topology 44 (2005) 1281–1300 MR

[64] **J Rasmussen**, **S D Rasmussen**, *Floer simple manifolds and L–space intervals*, Adv. Math. 322 (2017) 738–805 MR

[65] **S D Rasmussen**, *L–space intervals for graph manifolds and cables*, Compos. Math. 153 (2017) 1008–1049 MR

[66] **R Riley**, *A personal account of the discovery of hyperbolic structures on some knot complements*, Expo. Math. 31 (2013) 104–115 MR

[67] **S M Rump**, *Verification methods: rigorous results using floating-point arithmetic*, Acta Numer. 19 (2010) 287–449 MR

[68] **S Sarkar**, **J Wang**, *An algorithm for computing some Heegaard Floer homologies*, Ann. of Math. 171 (2010) 1213–1236 MR

[69] **H Segerman**, *A generalisation of the deformation variety*, Algebr. Geom. Topol. 12 (2012) 2179–2244 MR

[70] **A J Sommese**, **J Verschelde**, **C W Wampler**, *Introduction to numerical algebraic geometry*, from "Solving polynomial equations" (A Dickenstein, I Z Emiris, editors), Algorithms Comput. Math. 14, Springer (2005) 301–335 MR

[71] **M Soos**, *CryptoMiniSat, an advanced SAT solver* (2016) Version 5.0 Available at `https://github.com/msoos/cryptominisat`

[72] **W Stein**, et al., *SageMath mathematics software* (2018) Version 8.3 Available at `http://www.sagemath.org`

[73] **W P Thurston**, *Geometry and topology of three-manifolds*, lecture notes (1980) Available at `http://library.msri.org/books/gt3m`

[74] **W P Thurston**, *Three-dimensional geometry and topology, I*, Princeton Math. Ser. 35, Princeton Univ. Press (1997) MR

[75] **M Trnková**, *Rigorous computations with an approximate Dirichlet domain*, Topology Appl. 268 (2019) art. id. 106900 MR

[76] **J Verschelde**, *Algorithm 795: PHCpack: a general-purpose solver for polynomial systems by homotopy continuation*, ACM Trans. Math. Softw. 25 (1999) 251–276

[77] **J Verschelde**, et al., *PHCpack: solving polynomial systems via homotopy continuation* (1999) Available at `http://math.uic.edu/~jan`

[78] **J Weeks**, *Computation of hyperbolic structures in knot theory*, from "Handbook of knot theory" (W Menasco, M Thistlethwaite, editors), Elsevier, Amsterdam (2005) 461–480 MR

[79] **B Zhan**, *bfh_python: computations in bordered Heegaard Floer homology* (2014) Python package Available at `https://github.com/bzhan/bfh_python`

[80] **C K Zickert**, *Ptolemy coordinates, Dehn invariant and the A–polynomial*, Math. Z. 283 (2016) 515–537 MR

Department of Mathematics, University of Illinois at Urbana-Champaign
Urbana, IL, United States

`nmd@illinois.edu`

`http://dunfield.info`

Proposed: Cameron Gordon
Seconded: Rob Kirby, Ian Agol

Received: 9 April 2019
Accepted: 27 October 2019